GROWTH AND CHARACTERIZATION OF InSe SINGLE CRYSTALS

A THESIS SUBMITTED TO
THE GRADUATE SCHOOL OF NATURAL AND APPLIED SCIENCES
OF
MIDDLE EAST TECHNICAL UNIVERSITY

BY

DERYA DENİZ

IN PARTIAL FULFILLMENT OF THE REQUIREMENTS

FOR

THE DEGREE OF MASTER OF SCIENCE

IN

PHYSICS

AUGUST 2004

Approval of the Graduate School of Natural and Applied Sciences.

Prof. Dr. Canan Özgen
Director

I certify that this thesis satisfies all the requirements as a thesis for the degree of Master of Science.

Prof. Dr. Sinan Bilikmen
Head of Department

This is to certify that we have read this thesis and that in our opinion it is fully adequate, in scope and quality, as a thesis for the degree of Master of Science.

Assoc. Prof. Dr. Mehmet Parlak
Co-Supervisor

Prof. Dr. Bülent G. Akınoğlu
Supervisor

Examining Committee Members

Prof. Dr. Raşit Turan (METU, PHYS) _____

Prof. Dr. Bülent G. Akınoğlu (METU, PHYS) _____

Assoc. Prof. Dr. Mehmet Parlak (METU, PHYS) _____

Assoc. Prof. Dr. Mehmet Çakmak (GU, PHYS) _____

Assoc. Prof. Dr. Akif Esendemir (METU, PHYS) _____

I hereby declare that all information in this document has been obtained and presented in accordance with academic rules and ethical conduct. I also declare that, as required by these rules and conduct, I have fully cited and referenced all material and results that are not original to this work.

Name, Lastname: Derya Deniz

Signature :

ABSTRACT

GROWTH AND CHARACTERIZATION OF InSe SINGLE CRYSTALS

Deniz, Derya
Ms., Department of Physics
Supervisor: Prof. Dr. Bülent G. Akınoğlu
Co-Supervisor: Assoc. Prof. Dr. Mehmet Parlak

August 2004, 66 pages.

In this study, InSe single crystals were grown from the melt using conventional Bridgman-Stockbarger system. The grown crystals were implanted by N-ions to investigate the doping effect. The stoichiometry and the structural features were examined by scanning electron microscope and X-ray diffraction method, respectively. We have observed that the ingot was stoichiometric and the structure was hexagonal. Temperature dependent conductivity and Hall effect measurements were carried out to investigate the electrical properties of as-grown, as-implanted and annealed samples within the temperature range of 80-400 K. To investigate the annealing effect on both the absorption and photoluminescence (PL) spectra, absorption and PL measurements were performed at room temperature.

N- implantation reduced the resistivity order from 10^3 to 10^1 (Ω-cm). We have used temperature dependent conductivity and Hall effect measurements to analyze the dominant scattering mechanisms. Hall measurements showed that all the samples had n-type conduction.

Absorption measurements showed that InSe had direct band gap. It was observed that annealing had almost no effect on both room temperature absorption and PL spectra of the samples.

Keywords: Bridgman technique, InSe, ion implantation, electrical characterization, optical characterization.

ÖZ

InSe TEK KRİSTALLERİNİN BÜYÜTÜLMESİ VE KARAKTERİZASYONU

Deniz, Derya
Yüksek Lisans , Fizik Bölümü
Tez Yöneticisi: Prof. Dr. Bulent Akinoglu
Ortak Tez Yöneticisi: Assoc. Prof. Dr. Mehmet Parlak

Ağustos 2004, 66 sayfa.

Bu çalışmada InSe tek kristalleri konvansiyonel 3-bölmeli Bridgman-Stockbarger sistemi kullanılarak büyütüldü. Katkılama etkisini gözlemlemek amacıyla, büyütülen kristallere N-iyonlari ekildi. Elektron mikroskobu ve X-ışını kırınım cihazı kullanılarak, kristallerin tamkatlılığı ve yapısal özellikleri incelendi. Örneklerin elektriksel özellikleri, 80-400 K sıcaklık aralığında iletkenlik ve Hall etkisi deneyleri yapılarak incelendi. Tavlama sıcaklığının optik soğurma ve fotoışıma tayflarına etkisini gözlemlemek amacıyla optik soğurma ve fotoışıma ölçümleri oda sıcaklığında yapıldı.

N iyonları ekilmiş kristallerin özdirençlerinin 10^3 ten 10^1 Ω-cm'ye düştüğü gözlendi. Etkin saçılma mekanizmalarını belirlemek amacıyla sıcaklık bağımlı iletkenlik ve Hall etkisi deneyleri yapıldı. Bu ölçümlerden, örneklerin n-tipi yarıiletkenler gibi davrandıkları gözlendi.

Optik soğurma ölçümünden, InSe tek kristalinin direkt bant aralığına sahip olduğu gözlendi. Tavlamanının oda sıcaklığındaki optik soğurma ve fotoışıma tayfları üzerinde önemli etkileri olmadığı saptandı.

Anahtar Sözcükler: Bridgman tekniği, InSe, iyon ekme, elektriksel karakterizasyon, optik karakterizasyon.

To My Family...

ACKNOWLEDGMENTS

I express my deepest appreciation to my supervisor, Prof. Dr. Bülent G. Akınoğlu for his guidance and support during this study. I also thank to my co-adviser Assoc. Prof. Dr. Mehmet Parlak for his great effort and support throughout this work.

I would like to thank Prof. Dr. Hüsnü Özkan for the discussions we had during the x-ray analysis of the samples.

I am also grateful to Prof. Dr. Raşit Turan for his help and laboratory opportunity.

Special thank goes to Orhan Karabulut who helped me very much in the course of this study.

I wish also thank to Berna Serdar for her invaluable understanding, friendship, encouragement and support.

TABLE OF CONTENTS

LIST OF TABLES

LIST OF FIGURES

CHAPTER 1

INTRODUCTION

1.1 Introduction

According to their electrical properties, all the elements are classified in three main groups, named as conductor, insulator and semiconductor. A semiconductor material is neither a good conductor of electricity nor a good insulator. Electrical or even most physical and optical properties of semiconductors can be changed at a given temperature over several orders of magnitude by external means. Perfect crystal of most semiconductors behaves like an insulator at absolute zero. The characteristic semiconducting properties can be modified by thermal agitation, photonic excitation, impurities, lattice defects, or lack of stoichiometry (departure from nominal chemical composition)[1].

Quantum mechanical properties of matter basically determine the differences between semiconductors, metals, and insulators. The difference essentially arise from the fact that the atoms have only certain discrete values of energy called energy states or energy levels which are unique for each chemical element. In a solid material, these energy levels split into many close energy levels to accommodate the uppermost electrons forming allowed energy bands as well as a forbidden energy gap over a valance band. If the allowed energy bands are either completely

filled by electrons or empty, then the material behaves as an insulator since no electrons can be moved to an almost free band by the applied electric field. If the bands are partly filled the crystal will act as a metal since the electrons can be easily moved by the applied field to conduct current. In a semiconductor, one or two bands are slightly filled or slightly empty whereas all the others are entirely filled so that the material properties can be enhanced easily by some external means. The highest band is called the conduction band and has mostly empty energy states while the band just below the conduction band is called the valance band and mostly filled. The difference between the valence band and the conduction band is called the band gap energy or the energy gap. The value and the structure of the band gap in semiconductors are very important since they determine most of the physical properties of the material and by modifying this structure different electronic devices for application can be fabricated such as; transistors, rectifiers, modulators, detectors, thermistors, and photocells [1,2].

In a pure neutral ideal semiconductor, the concentration of negatively charged electrons must be equal to the concentration of positively charged holes. In this case, the semiconductor is said to be intrinsic. However, electron and hole concentrations can be changed by adding the impurity atoms to the semiconductor. These impurities are called donors (or n-type dopants) and acceptors (or p-type dopants), respectively. Doped semiconductors are called extrinsic semiconductors. Donors introduce energy levels into the energy gap that are close to the bottom of the conduction band. These energy levels are called donor levels. Acceptors introduce energy levels into the energy gap that are above and close to

the valence band. These energy levels are called acceptor levels. A semiconductor is called an n-type semiconductor if it is doped with donors. A semiconductor is called a p-type semiconductor if it is doped with acceptors. When both donors and acceptors are introduced to a semiconductor, these donors and acceptors compensate each other, since electrons generated by donor levels tend to occupy the vacant levels in the valence band created by the acceptor agents. In this case, the semiconductor is called compensated. In a compensated semiconductor, the larger impurity concentration makes the semiconductor either n-type or p-type [2].

The semiconductors listed in column IV and neighboring columns of the periodic table are the elemental semiconductors since they consist of single species of atoms. The compounds of columns III-V, II-VI and III-VI, make compound semiconductors.

Many investigations have been carried out about the III-VI compound semiconductors, especially InSe, GaSe, InS, GaTe and GaS which are the compounds between metals (In, Ga) and the chalgogens (Se, S, Te) and named as In- and Ga-chalgogens. These compound semiconductors have layered or chain structures. The basic unit consists of two planes of metal atoms sandwiched between two planes of chalgogen atoms [3]. Atoms are bound by a mixture of covalent and ionic bonds within a layer, while the interlayer bonding is due to the weaker van der Waals forces. Combinations of these strong and weak bonds cause asymmetric charge distributions around the atoms [4].

Considerable attention has been paid to the study of the layered III-VI compound InSe due to its possible applications in photo-electronic devices [5]. In layered semiconductors, dangling bonds do not exist on the surfaces perpendicular to c-axis which can be easily obtained by cleaving from the crystal ingot. Low density of dangling bonds together with its suitable electrical and optical properties makes InSe an attractive material for application in photovoltaic conversion [6]. Using Bridgman-Stockbarger systems, InSe single crystals can be grown as both n and p type depending on growth conditions and dopant elements. As stated above, optical and electrical properties of a crystal can be adjusted by doping method. Doping may be achieved by chemical process which is essentially direct addition of the dopant elements into the growth ampoules. However, in this method, it is not easy to control the amount of impurity in the crystal due to solubility problems and segregation [7, 8]. In this thesis, we have used ion implantation technique knowing that this technique does not render the difficulties mentioned above. In ion implantation method, the sample is placed in a vacuum chamber and bombarded by a beam of highly energized ions in the energy ranges from keV to MeV. This technique is very advantageous since dopant atoms can be implanted in various concentrations regardless of their solubility in the bombarded material.

1.2 Crystal structure of InSe

InSe is a layered compound and a member of the III-VI semiconductor family. Our as-grown undoped InSe is an n-type semiconductor with band gap energy of

about 1.2 eV at room temperature and a melting point at 660^oC. The structure of InSe crystal is close-packed hexagonal which contains four mono-atomic layers in the sequence of Se-In-In-Se [9]. The bonding within each layer is predominantly covalent whereas the layers are hold by weak Van der Waal's forces that results in easy cleavage perpendicular to c-axis [10]. As we previously stated, the strong bonding inside the planes and weak van der Waals bonding between the layers cause anisotropy because of the asymmetric charge distributions around the atoms. As a result of anisotropic bonding, there are three different polytypes denoted as ϵ, β, and γ depending on growth parameters. These are specified by different stacking sequences of four fold atomic layers.

In the literature, InSe is described with two different structural modifications, corresponding to a γ and ϵ or β polytypes [10]. The crystals grown from a non-stoichiometric melt using Bridgman-Stockbarger technique show the hexagonal structure belonging to the ϵ or β structural modifications [11]. It was reported that the atoms inside each plane of InSe are arranged in rhombohedral or hexagonal modifications and the c-axis is perpendicular to the surfaces of the cleaved samples [10, 11]. Fig.1.1 shows undoped InSe single crystal that has been grown in our laboratory using Bridgman system. The orientation of the crystal can easily be seen at the bottom of the ingot.

1.3 Previous studies concerning InSe single crystals

InSe has been extensively studied with respect to its optical properties [12, 13, 14, 15, 16], electrical properties [17, 18, 19], growth techniques and structural

Figure 1.1: InSe single crystal ingot grown from a non-stoichiometric melt using Bridgman-Stockbarger technique in our laboratory.

properties [6, 9, 10, 11, 20, 21].

It is possible to grow good quality single crystals from non-stoichiometric melts using Bridgman and Czochraski techniques. Small samples can also be grown by the vapor phase and chemical transport [10]. A. Chevy et al. [21] stated that crystal growth from the vapor phase (sublimation or transport) or from the liquid stoichiometric phase (Bridgman, zone fusion, directional freezing) does not allow the growth of large InSe single crystals. The most conventional technique to grow good quality single crystals is the Bridgman method. The details of this technique are given in chapter 2 and chapter 3.

C. De Blasi et al. [9] grew high quality InSe monocrystals from nonstoichiometric melt using Bridgman-Stockbarger method. In their study, the structure of InSe was reported to be hexagonal. In order to obtain information about the

resistivity and mobility variation with temperature for InSe, they carried out measurements over the temperature range 100-300 K. They found that the analyzed samples had n-type conductivity in the temperature range investigated. In their study, the room temperature resistivity ranged between 10^2 and 10^4 Ω-cm and the room temperature Hall mobility was reported to be between 10 and 500 cm^2/Vs.

S. Shigetomi et al. [17] studied the annealing effects on the temperature dependencies of the electron concentration and the Hall mobility. In their paper, the results of annealing effects on the electron concentration of undoped InSe showed that the thermal ionization energy of the donor level is 23 meV and is independent of annealing temperature. They concluded that the ionized impurity scattering becomes dominant in the scattering mechanism of electrons in n-type InSe as the annealing temperature of the samples increases.

C. De Blasi et al. [18] carried out a systematic study on the electrical properties of undoped n-type InSe grown from melt by performing resistivity, Hall-effect and space-charge-limited-current (SCLC) measurements over the range between 100 and 300 K. They found that the two donor levels at about 0.10 and 0.34 eV below the conduction band dominated the electrical properties of the investigated samples. In their paper, they reported that the 0.34-eV donor, if partially compensated, gives rise to an electron- trapping center that influences the SCLC at room temperature.

Savitskii et al. [15] have studied space-charge region scattering mechanisms of undoped n-type InSe in the temperature range between 80 and 400 K. They

have shown that the Hall mobility ranged from 600 to 750 cm^2/Vs in the samples with low room temperature and the temperature dependence of $\mu_H(T)$ could be explained by electron scattering on charged impurity aggregates surrounded by space-charge regions. They observed that in a certain temperature range around a critical value T_0, the mobility dependence along the layers is like $\mu = \mu_0(T/T_0)^{-\gamma}$, where γ depends on the phonon energy and the dimensionality of the electron gas. In the samples with carrier concentration from $n \sim 10^{15}$ to $10^{16}cm^{-3}$, they found that the Hall mobility is in the range between $\mu_H = 850$ and $1000cm^2/Vs$ at 300 K with the exponent γ to be in the range of 1.6 to 2.1 (depending on the impurity content). Below room temperature they observed shallow donors with activation energy of 12 to 16 meV. Above room temperature they found deep donors with an activation energy of 0.45 eV and a concentration of $2.5\times10^{17}cm^{-3}$. In their study, it has been observed that at higher temperatures the Hall mobility is controlled by phonon scattering mechanism with 14.3 meV phonon energy, whereas at lower temperatures it is limited by impurity scattering.

Some researchers have also studied the optical and electrical properties along and perpendicular to c-axis, since layered crystals are characterized by strong anisotropy in most of their physical properties. In their article, Savitskii et al. [19] reported the temperature dependencies of the conductivity of InSe along and perpendicular to c-axis in the range from 80 to 400 K. From the conductivity measurements, they observed a lower conductivity value along the c-axis than along the layers. They concluded that the anisotropy ratio $\sigma_{\perp c}$ / $\sigma_{\parallel c}$ is temperature-independent and has small value (≈ 2) for crystals of high quality.

C. De Blasi et al. [13] studied photoconductivity of this layered compound. They observed a strong thermal quenching of photoconductivity at various excitation levels. In their study the relation between photocurrent ($\triangle_{ph}$) and exciting light (L) intensity was reported as $\triangle_{ph} \sim L^2$. From the analysis of the thermal quenching, they reported a level at 0.20 eV above the valance band which behaves as trapping or recombination center depending on the temperature and the excitation intensity. They concluded that InSe is a good photoconductor.

A. A. Homs et al. [22] examined the photoluminescence spectra of this compound in the range of 15-280 K under different excitation power densities. They observed that narrow peaks between 1.30 and 1.34 eV characterize InSe. It was reported that there is an exciton bound to the native donor with energy E_D =19 meV. They explained the temperature dependence of the free exciton energy in terms of the band gap energy shift and the exciton line broadening, where scattering by acoustic phonons is important at low temperatures.

As we stated previously, Indium monoselenide can be grown as both n and p type depending on growth conditions and dopant elements introduced during the growth process. The Bridgman grown undoped stoichiometric InSe is n-type. Many researchers have been studied InSe doped with different elements by introducing the impurities directly to the growth ampoule. It was seen that p-type conductivity can be obtained by doping the material with chemical impurities such as Hg [5], Zn [23], Cd [24], Sb [25], As[26], P [27], and N [28] while InSe showed n-type conductivity when it is doped with I [29], Er [30], Sn [31], and Si [32].

S. Shigetomi et al. [5] examined the impurity levels in p-type InSe doped with Hg by photoluminescence (PL) and Hall-effect measurements. They observed a broad emission band at 1.237 eV (77 K) on the PL spectra of samples doped with Hg in the range 0.02 to 0.1 at percentage. It was reported that the PL intensity increases with increasing Hg concentration and this comes from the recombination between the donor level and the acceptor level at 0.07 eV above the valance band. They concluded that the position of the acceptor level obtained from PL measurements is in agreement with the results of Hall effects.

Micocci et al. [23] investigated the deep levels in p type InSe single crystals doped with Zn by resistivity, Hall-effect, photoinduced-current transient spectroscopy (PICTS) and space-charge-limited-current (SCLC) measurements. They concluded that the carrier transport is dominated by an acceptor level with an activation energy of about 0.59 eV above the valance band and with a density that depends on the amount of the Zn included in the starting charge before growing the single crystals. They observed one hole trapping center between 0.56 and 0.60 eV above the valance band by using PICTS and SCLC measurements and these values of energy were in agreement with the activation energy of accepter center obtained by Hall-effect measurements.

G. Micocci et al. [24] examined the electrical properties of p type InSe doped with Cd through resistivity, Hall-effect and deep-level transient spectroscopy (DLTS) measurements. They have concluded that the short-range interaction with the homopolar optical phonon is the dominant scattering mechanism limiting the Hall mobility in this compound semiconductor at higher temperatures,

whereas the mobility behavior is consistent with an ionized-impurity scattering mechanism at lower temperatures. In their article, it was reported that the carrier transport of Cd-doped InSe is dominated by the acceptor level at about 0.47 eV above the valance band and with a concentration that depends on the amount of the doping material included in the charge before growing the crystals. They have observed two hole trapping centers at 0.42 and 0.48 eV above the valance band using DLTS measurements.

S. Shigetomi and T. Ikari [25] have investigated the optical and electrical characteristics of layered semiconductor p-InSe doped with Sb by performing photoluminescence (PL), Hall-effect and optical absorption measurements. They have observed the emission band at 1.02 eV in the PL spectra of the samples doped with 0.05 to 0.5 at percentage Sb. From the dependence of the excitation intensity of the PL intensity and peak energy, they found that the 1.02 eV emission band is due to the transition related to a donor-acceptor pair. They detected that the deep acceptor level located approximately 0.4 eV above the valence band using the Hall-effect and optical absorption measurements. They concluded that the deep acceptor level is probably associated with the defects formed by Sb atoms in the interlayer.

G. Micocci et al. [26] examined the impurity levels in As-doped p-InSe by Hall-effect and deep-level transient spectroscopy (DLTS) measurements. In their study, they found one hole trapping center located at about 0.57 eV above the valance band from DLTS measurements. They concluded that this center can be identified with the deep level obtained by Hall-effect measurements. They

observed that the intensity of DLTS peak depends on the amount of As included in the melt before growing the crystals.

G. Micocci et al. [27] performed deep-level transient (DLTS) measurements on P-doped p-type InSe. They observed that all the InSe samples to be p-type with a Hall mobility at room temperature of the oder of 5 to 10 cm^2/Vs and a resistivity ranging between 10^2 and 10^5 Ωcm. In their article, they found that the height of the DLTS peak is enhanced with increasing P concentration.

F. J. Manjon et al. [28] reported on photoluminescence (PL) measurements under pressure on p-type N-doped InSe at 10 K. They observed that low-temperature PL of N-doped InSe is dominated by a band-to-acceptor peak at 1.289 eV and its one phonon replica at 1.264 eV.

G. Micocci et al. [29] studied the deep levels in n-type InSe single crystals doped with Iodine through deep-level-transient spectroscopy (DLTS) measurements. They found that there are two trap levels located at about 0.60 and 0.21 eV below the conduction band. They concluded that the electron trap located about 0.60 eV is also present in undoped n-InSe crystals, while the trapping levels at 0.21 eV can be due to incorporation of Iodine since it is always present in doped n-InSe samples.

M. Yildirim et al. [30] performed Hall-effect measurements on n-type InSe doped with Er in the temperature range 10-340 K. In their study, it was reported that the carrier concentration in the Er doped InSe increases up to 300 K. In the same samples, they observed that the Hall mobility decreases up to 340 K and obeys to $\mu_H = T^{-1.51}$ for T $>$ 80 K.

S. Shigetomi et al. [31] investigated the impurity levels of n-type InSe doped with Sn by photoluminescence (PL) and Hall-effect measurements. They observed that the carrier transport in the Sn-doped n-type sample is governed by the donor level at 0.06 eV below the conduction band and this donor level is related to the radiative recombination of the 1.27 eV emission band.

J. Riera et al. [32] carried out photoluminescence (PL) measurements on Silicon doped n-type InSe. They have studied the effect of temperature and excitation intensity in the range between 30 and 300 K. They reported free and neutral donor bound exciton peaks at low temperatures. They detected free exciton and band-to-band photoluminescence above 100K. They observed no compensating acceptor centers in Si-doped InSe.

As previously stated, we may not control the amount of impurity in chemical doping technique due to segregation and solubility problems. These problems are not encountered in ion implantation technique. V. V. Gridin et al. [33] studied temperature dependent photoluminescence of the Sn-implanted InSe, which is the only article that we found concerning implantation of InSe single crystals.

1.4 Present Study

In this thesis, we have grown indium monoselenide from non-stoichiometric melt using conventional Bridgman-Stockbarger method and examined its structural, electrical and optical properties. The effect of N-implantation on structural, electrical and optical properties has been investigated by means of X-ray diffraction, temperature dependent conductivity and Hall mobility measurements

over the temperature range of 80-400 K, absorption and photoluminescence measurements at room temperature. In the second chapter, some basic theoretical information for structural, electrical and optical properties of materials is given. In chapter 3, all the experimental steps required to grow a layered compound and also the measurements techniques are mentioned. The experimental results from the X-ray, electrical and optical measurements are given in chapter 4 together with the discussions. Lastly, in chapter 5, the conclusions of the results have been presented.

CHAPTER 2

THEORETICAL APPROACH

2.1 Introduction

In this chapter, material growth techniques are summarized. Theoretical background and necessary information required for the structural, electrical and optical characterizations of the grown and doped samples are also given in this chapter.

Crystal growth techniques can be divided into two groups which are bulk material growth and epitaxial growth. The controlled growth of crystalline material onto single crystal surfaces of different materials is named epitaxial growth. Epitaxial growth is the growth of single crystal thin film on the surface of the same material or another one [34]. In this technique, the substrate is used as the seed crystal onto which another crystalline material is grown. The new growing crystal layers keep the orientation and structure of the used substrate. Millions of devices are fabricated using this technique [2]. There is a great variety of methods for epitaxial deposition of different materials. Chemical Vapor Deposition (CVD), Liquid Phase Epitaxy (LPE), Atomic Layer Epitaxy (ATE), Molecular Beam Epitaxy (MBE), Metal Organic Chemical Vapor Deposition (MOCVD), Low Pressure Metal Organic Chemical Vapor Deposition (LP-MOCVD) and Metal

Organic Molecular Beam Epitaxy (MOMBE) are among the most widely used methods [34].

In a Molecular Beam Epitaxy (MBE) system, a deep vacuum is maintained inside the MBE chamber, and a heated semiconductor substrate is coated by evaporating the desired material. Then, a high-quality semiconductor film is formed on the substrate. MBE growth is very slow process with typical rates on the order of 10 nm/min and MBE machines are very expensive [2].

Chemical Vapor Deposition (CVD) and Liquid Phase Epitaxy (LPE) are preferred when mass production of semiconductor devices is desired. In a chemical vapor deposition system, gases of the elements are passed through a substrate held at high temperatures. Chemical reactions on the surface result in a growth of the desired structure. In LPE process, a semiconductor substrate is put in contact with a semiconductor melt for a strictly controlled period of time, resulting in a deposition of an epitaxial film [2].

Metal Organic Chemical Vapor Deposition (MOCVD) is another CVD process. MOCVD utilizes organic compounds incorporating semiconductor and dopant atoms. This technique can be combined with MBE.

In Bridgman-Stockbarger technique, zone melting technique, Czochralski and Kyropoulos techniques, the crystals are grown from the melt. In order to use these techniques, the compounds which have a low pressure at the melting point should be used. For compounds with high vapor pressures, some modifications are required.

The Bridgman-Stockbarger technique is a directional solidification process.

Either the crucible (Bridgman) or the temperature gradient (Stockbarger) can be moved. In Bridgman method, a crucible containing a melt is lowered from an upper high temperature zone into a lower temperature zone. As the crucible is moved downward through the cooling isotherm nucleation occurs at the tip and crystallization proceeds vertically. The principles of this technique were given in details in the next chapter.

In the zone melting technique, a heating element is passed several times over the material so that in each passage many impurities prefer to stay in the melt leaving better crystals. If a seed crystal is included in the apparatus, the method is called as Floating-Zone method.

The pulling of crystals from their melts is used when relatively large perfect crystals are desired to grow. In Czochralski and Kyropoulos techniques, the melt is contained in a crucible but the crystal is grown at the free top surface of the melt so that there is no need to put the charge into a crucible which may reduce the contamination. In Czochralski method, the crystal is pulled from a melt by touching a seed substrate to the surface. In this method the heat supply must be kept reasonably constant. However, in Kyropoulos method, the crystal grows into the melt as the heat flow to the melt is decreased. In latter method, controlling the shape of the crystal may be diffucult and there might be some problems due to the thermal shock when the crystal is finally removed from the melt [35].

2.2 Doping Techniques

The optical and electrical properties of semiconductors can be modified by means of introducing the impurities into the crystals. This process is named as doping. If the impurity introduces additional hole (or electron) then the impurity is called as acceptor (or donor). Doping process can be either chemical or implantation. In the chemical doping process, dopant element is directly added to the growth ampoule. The impurity concentration is usually very small. The chemical doping method renders some difficulties such as solubility and segregation of the dopant agents in the host material [7, 8].

In ion implantation technique, the semiconductor sample is bombarded by ions having energy between the keV and MeV ranges. These ions usually damage the surface layer by penetrating. The penetration depth depends on the implanted species and on the ion energy. After the implantation, the sample is heated and kept for some time at a fairly high temperature to possibly remove the damage introduced by ion implantation and also for a deeper penetration. This technique is very advantageous since the doping agents can be implanted in different concentrations regardless of their solubility and segregation in the host material [2, 7, 8].

2.3 Crystal Structure Determination

The determination of an unknown structure can be completed by following three main steps. Firstly, the size and shape of the unit cell can be obtained

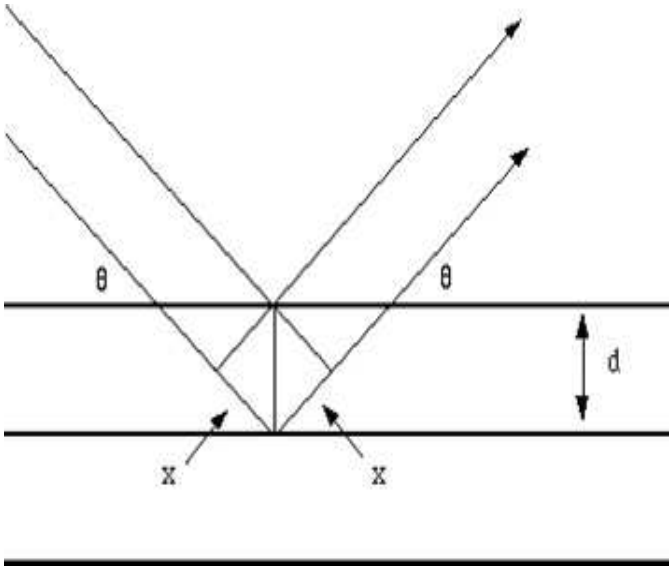

Figure 2.1: Reflections From Atomic Planes.

from the angular positions of the diffraction lines. After choosing the correct crystal system, the correct Miller indices can be assigned. Once this is achieved, the shape of the unit cell and its size are deduced from the positions and Miller indices of the diffraction lines. The number of atoms included within a unit cell is then computed from the size and shape of the unit cell. Lastly, the atomic positions in the unit cell are deduced from the relative intensities of the diffraction lines [36].

X-rays having wavelengths comparable with the distance between the atomic planes in a crystal structure is diffracted by the atomic planes. Therefore, the resulting diffractograms can be used to determine the structure of the crystals [36].

Fig.2.1 shows the reflections from different atomic planes. Phase relations

Table 2.1: The variations of λ and θ in three main diffraction methods

Method	λ	θ
Laue Method	variable	fixed
Rotating Crystal Method	fixed	variable
Powder Method	fixed	variable

between two or more waves create diffraction. Differences in phase lead to differences in path-length of rays reflected from different atomic planes resulting in either a constructive or a destructive pattern.

Diffraction maxima can occur whenever the Bragg law

$$n\lambda = 2d\sin\theta \tag{2.1}$$

is satisfied. In this equation, n is a positive integer and shows the order of reflection maximum, λ is the wavelength of the X-rays, d is the spacing between atomic planes in the crystal and θ is the angle between the normal to the atomic plane both for the incident and reflected beams. The ways in which these quantities are varied introduce the three main diffraction methods which are the Laue method the rotating crystal method and the powder method. Table 2.1 shows how these quantities are varied in these methods.

In this study, we used both the powdered and bulk samples for structural analysis. In X-ray analysis, the intensities and positions of the diffraction maxima are found to identify the structure of the crystals. Information about the size, cell parameters, space group and orientation can be deduced from the analysis of the diffraction maxima [36]. A monochromatic X-ray beam is directed onto powdered and bulk samples. In powder, the planes of the crystal are randomly oriented with respect to the beam direction. Diffraction maxima occur according

to Bragg law. Since λ is fixed, there will be constructive interference observed at definite angle due to reflection from crystal planes which are oriented to satisfy Bragg law.

To analyze the data obtained from the X-ray measurements, we have used an indexing program, TREOR 90. This program is written in Fortran by Werner et al [37]. The program involves separate routines for cubic, tetragonal, hexagonal, orthorhombic, monoclinic and triclinic symmetries. TREOR 90 searches for the solutions in index space by altering the Miller indices. The over all success rate of the program has been known to be more than 90 percent.

2.4 Electrical Characterization

Electrical characterization can be achieved by conductivity and Hall-effect measurements. Conductivity measurements give information about the nature of impurities and/or defects which are generally the sources of the trapping levels within the band gap region. Hall-effect measurements are widely used in the characterization of semiconductor materials since it is possible to get some information on the mobility, scattering mechanisms and carrier concentrations of the investigated samples.

In practice, the electrical characterization of a semiconductor is performed through temperature dependent conductivity and Hall-effect measurements. Semiconductors have no charge carriers at 0 K. If the temperature of a semiconductor is risen above 0 K, some electrons in the valance band are thermally excited to the conduction band. This process results in accommodation of some electrons

in the conduction band while holes remain in the valance band. These electrons and remaining holes are called electron-hole pairs (EHP).

Electrons in a solid obey Fermi-Dirac statistics. In Fermi-Dirac distribution, the probability of occupancy is given by an expression as [2];

$$f_n(E) = \frac{1}{1 + e^{(E-E_f)/kT}} \tag{2.2}$$

where E_f is called the Fermi energy (or Fermi level) and k is the Boltzman constant. If the Fermi level is given, then the total electron concentration within the conduction band can be found by evaluating the following integral equation;

$$n = \int_{E_c}^{\infty} f_n(E) g_n(E) dE \tag{2.3}$$

where g_n(E) is the density of available states and E_c is the energy of the conduction band edge. This integral equation can be simplified as;

$$n = N_c f(E_c) \tag{2.4}$$

where N_c is an effective density of states [2]. N_c represents all the states that are accessible in the conduction band edge.

For the edge of the valance and conduction band, the effective density of states can be written as [2];

$$N_v = 2(\frac{2\pi m_p kT}{h^2})^{3/2} \tag{2.5}$$

and

$$N_c = 2(\frac{2\pi m_n kT}{h^2})^{3/2} \tag{2.6}$$

respectively. If it is assumed that E_c-E_f and E_f-E_v are several times larger than thermal energy kT, then the semiconductor is said to be nondegenerate and the Fermi function is reduced to an exponential form as [2] :

$$f(E) = e^{-(E_c - E_f)/kT}. \tag{2.7}$$

Using Eqn.(2.4) one can get the electron concentration in the conduction band as follow;

$$n = N_c e^{-(E_c - E_f)/kT}. \tag{2.8}$$

Using the same considerations, the hole concentration in the valance band can be given as;

$$p = N_v e^{-(E_f - E_v)/kT}. \tag{2.9}$$

As long as the thermal equilibrium is maintained, these electron Eqn.(2.8) and hole concentrations Eqn.(2.9) are valid for all intrinsic and extrinsic crystals. In intrinsic materials, the Fermi level E_f lies at the same intrinsic energy level E_i near the middle of the band gap energy. Then, the intrinsic electron and hole concentrations are;

$$n_i = N_c e^{-(E_c - E_i)/kT} \tag{2.10}$$

and

$$p_i = N_v e^{-(E_i - E_v)/kT} \tag{2.11}$$

respectively.

The np product for a nondegenarate semiconductor does not depend on the position of the Fermi level and it is determined by the densities of states in the

conduction and valance bands, the band gap energy and the temperature. At thermal equilibrium the mass-action law can be expressed as follow [2];

$$n_i^2 = np. \tag{2.12}$$

2.4.1 Electrical Conductivity

The conductivity of a semiconductor is given as [2];

$$\sigma = q(\mu_n n_i + \mu_p p_i) \tag{2.13}$$

where q is the electron charge, n_i and p_i are the intrinsic density of free electrons and holes, and μ_n and μ_p are the electron and hole mobility, respectively. The hole contribution to the conductivity of an n-type semiconductor is often neglected since the hole concentration is many orders of magnitude smaller than the electron concentration. Likewise, the electron contribution to the conductivity of a p-type semiconductor can be neglected.

Considering an n-type semiconductor and substituting Eqn.(2.10) into Eqn.(2.13), one can obtain the following expression for the conductivity;

$$\sigma = N_c e \mu e^{-(E_c - E_i)/kT} \tag{2.14}$$

where μ is the mobility. From Eqn.(2.6) one can see that N_c is directly proportional to $T^{3/2}$. At low temperatures the mobility increases with temperature according to the law $\mu \sim T^{3/2}$. Such a behavior is characteristic of a scattering mechanism of charge carriers with ionized impurities. In the higher-temperature range the mobility decreases according to the law $\mu \sim T^{-3/2}$. In this range

the mobility is governed by a short-range interaction with a homopolar optical phonon polarized normally to the layers [18]. Thus, the conductivity expression at sufficiently high temperatures can be written as follow;

$$\sigma = \sigma_0 e^{-(E_c - E_i)/kT} \tag{2.15}$$

where σ_0 is a constant. In an intrinsic semiconductor, the Fermi level is located near the middle of the bandgap. If a semiconductor contains impurities then it has impurity energy levels. For extrinsic nondegenerate semiconductors, as the donor concentration gets higher then the Fermi level moves closer to the conduction band and shallow donors are present. Similarly, as the acceptor concentration gets higher then the Fermi level moves close to the valance band and shallow acceptors are present. Activation energy for the donor (or acceptor) E_D (or E_A) can be estimated by performing temperature dependent conductivity measurements. When the doping concentration is equal or larger than the corresponding effective density of states then the Fermi level is above the conduction band or below the valance band. In this case, there are many trapping levels are present in the material and the semiconductor is said to be degenerate.

2.4.2 The Hall-Effect

The physical principle governing the Hall-effect is the Lorentz force. If an electric current flows through a conductor in an applied magnetic field, the magnetic field exerts some transverse force on the moving charge carriers (holes or electrons). Thus, the charge carriers accumulate at one side of the conductor.

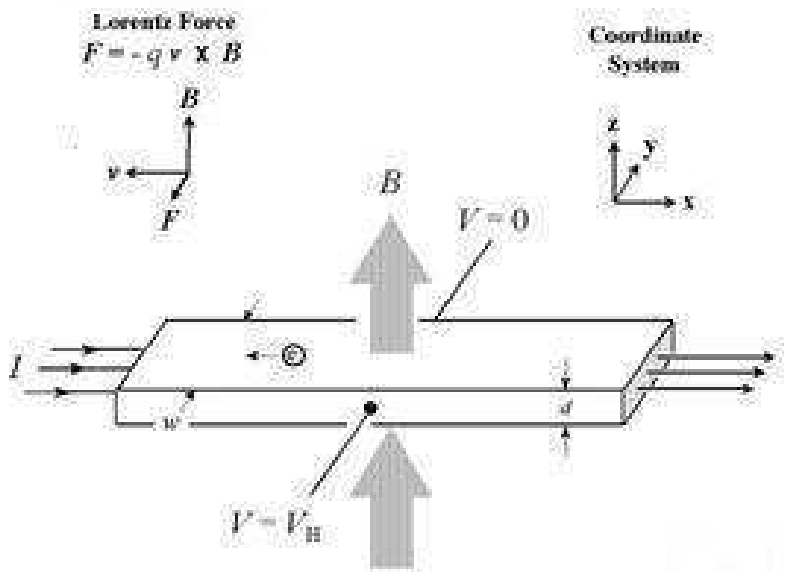

Figure 2.2: The Hall-Effect.

This magnetic influence is balanced by a measurable voltage between the two sides of the conductor. The presence of this measurable transverse voltage is called the Hall effect after E. H. Hall who discovered it in 1879. For an n-type, bar-shaped semiconductor shown in Fig.2.2, the total force on a single electron in the presence of the applied electric and magnetic field is expressed as;

$$\mathbf{F} = q[\mathbf{E} + \mathbf{v} \times \mathbf{B}] \tag{2.16}$$

If the current is constant and flows in the x-direction and the magnetic field is applied in the z-direction, then the current can be given by;

$$I = qwdnv_x \tag{2.17}$$

where, n is the electron concentration, v_x is the drift velocity, ω and d are width and thickness of the material, respectively. Electrons subject to the Lorentz force

initially drift away from the current line toward the positive y-axis, resulting in an excess surface electrical charge on the side of the sample. This charge results in the Hall voltage, a potential drop across the two sides of the sample. In the z-direction, there is no force on the electrons and therefore $F_z = 0$. Using Eqn.(2.16) and Eqn. (2.17), one can obtain the electric field as;

$$E_z = \frac{B_y I_x}{qwdn}. \tag{2.18}$$

Then, the Hall voltage V_H generated by the electric field in z-direction is;

$$V_H = -\frac{B_y I_x}{qdn}. \tag{2.19}$$

The Hall voltage is directly proportional to the product of the magnetic field flux and the current density. The proportionality constant $R_H = \frac{-r}{qn}$ is called as the Hall constant where r is the scattering factor. One can find the electron concentration by measuring the Hall voltage for a known magnetic field and current;

$$n = -\frac{1}{qR_H}. \tag{2.20}$$

For a p-type semiconductor, one can obtain the hole concentration as;

$$p = \frac{1}{qR_H}. \tag{2.21}$$

Resistivity and Hall measurements should be carried out to find both the mobility μ and carrier concentrations. The Hall mobility is expressed as [2];

$$\mu_H = |R_H \sigma|. \tag{2.22}$$

Temperature dependent Hall-effect and conductivity measurements are important in the electrical characterizations of the semiconductors since it is possible to find

the carrier concentrations and mobility from these measurements. Variation of the mobility with respect to temperature also gives information about the scattering mechanisms.

2.5 Optical Characterization

Absorption and photoluminescence (PL) measurements are widely used techniques in the optical characterizations of the materials. Band gap structure can be investigated by performing the temperature dependent absorption measurements. Impurity levels and concentrations in a semiconductor can be obtained through temperature dependent PL measurements.

Absorption spectrum of a semiconductor can be used to investigate its band gap structure. In this process, electrons are excited from lower to higher energy levels by photons of known energies. Absorption occurs if the photon energy is greater than the band gap energy while transmission is the case if the photon energy is smaller than the band gap energy. Thus, a photon with energy $h\nu \geq E_g$ can be absorbed by a semiconductor and then an electron is excited from the valance band to the conduction band. In this case, absorption refers to band-to-band transitions. The absorption coefficient can be given by the following expression [38];

$$\alpha(h\nu) = A \sum P_{if} n_i n_f \tag{2.23}$$

where A is the proportionality constant, P_{if} is the probability for the transition from the initial state to the final state, n_i is the density of the electrons in the

initial state and n_f is the density of available final states.

The transitions either direct or indirect are divided into two types which are allowed and forbidden transitions. In allowed direct transitions, P_{if} is independent of photon energy and conduction and valance bands are located at the same momentum level. Thus, the energy of the final state is expressed as [38];

$$E_f = h\nu - |E_i| \tag{2.24}$$

then the absorption coefficient can be written as;

$$\alpha(h\nu) = A^*(h\nu - E_g)^{1/2} \tag{2.25}$$

where A^* is the following expression;

$$A^* \approx \frac{q^2(2\frac{m_h^* m_e^*}{m_h^* + m_e^*})^{3/2}}{nch^2 m_e^*}. \tag{2.26}$$

However, in some materials, direct transitions are forbidden at k=0 and allowed at k≠0 due to the quantum selection rules, where k=p/ $\hbar$ is the wave vector and p is the momentum. Transition probability increases with k^2. Since the density of states is proportional to $(h\nu - E_g)^{1/2}$, the absorption coefficient can be written as follow [38];

$$\alpha(h\nu) = A^{'}(h\nu - E_g)^{3/2} \tag{2.27}$$

where $A^{'}$ is;

$$A^{'} \approx \frac{4}{3}\frac{q^2(\frac{m_h^* m_e^*}{m_h^* + m_e^*})^{5/2}}{nch^2 m_e^* m_h^* h\nu}. \tag{2.28}$$

In some materials, conduction and valance bands do not lie at the same momentum level. The transition between such bands is called indirect transition and

requires a change in both energy and momentum. Therefore, a double process is needed since photon can not create a change in momentum. Momentum actually conserved by phonon interaction. Thus, to complete the transition from E_i to E_f, a phonon with energy E_p is either emitted or absorbed. These two process are given by the following expressions [38];

$$h\nu_e = E_f - E_i + E_p \tag{2.29}$$

$$h\nu_a = E_f - E_i - E_p. \tag{2.30}$$

The number of phonons is given by Bose-Einstein statistics;

$$N_p = \frac{1}{exp(\frac{E_p}{kT}) - 1}. \tag{2.31}$$

The absorption can be found by taking the product of the number of phonons, the densities of initial states and final states. Thus, the absorption coefficient for a transition with phonon absorption is [38];

$$\alpha_a(h\nu) = AN_p(h\nu - E_g - E_p)^2 \tag{2.32}$$

for $h\nu > E_g - E_p$ and the absorption coefficient for a transition with phonon emission is;

$$\alpha_e(h\nu) = AN_p(h\nu - E_g + E_p)^2 \tag{2.33}$$

for $h\nu > E_g + E_p$.

Photoluminescence (PL) is widely used non-destructive technique for the optical characterization of semiconductors by the fact that it allows the determination of impurities and band gap energies of the materials. In this process, a photon

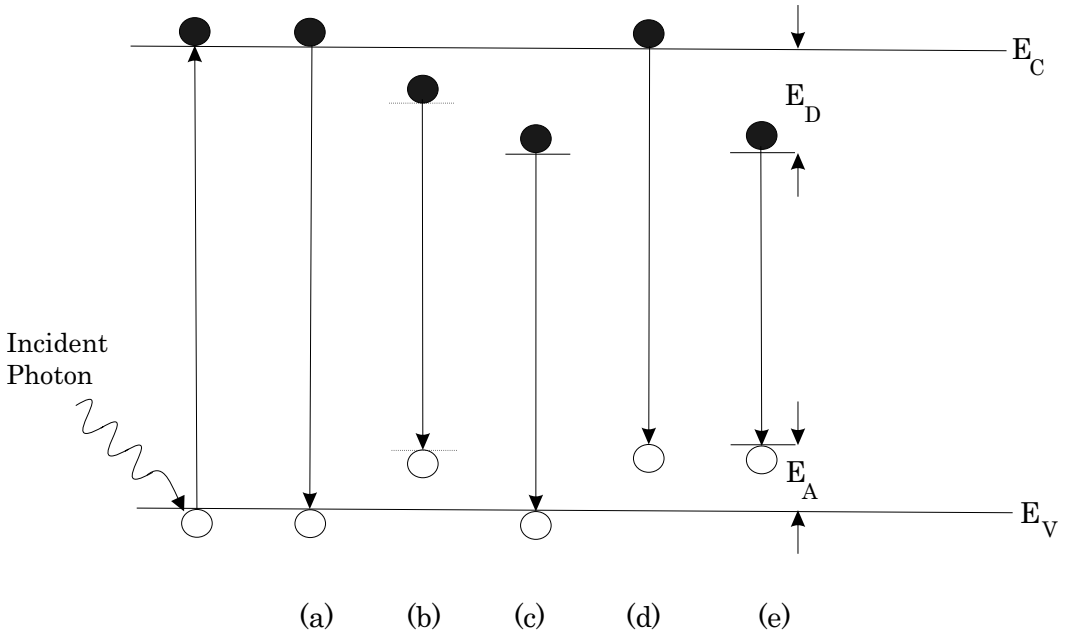

Figure 2.3: The most common five radiative transitions observed with photoluminescence.

with energy $h\nu \geq E_g$ is absorbed by the material, generating an electron-hole pair which then recombines, emitting another photon [38]. This process is radiative recombination and light emission occurs only in radiative recombination. Non-radiative recombination can not be detected in PL measurements. Performing temperature dependent PL measurements, one can determine the impurities. However, it is difficult to measure the concentration of impurities through PL measurements.

In PL process, the material is excited with a laser with energy $h\nu \geq E_g$ and then electron-hole pairs are generated. In order to have fine PL output, majority of the recombination process is to be radiative. Fig.2.3 illustrates most commonly observed five PL transitions.

The first transition described in Fig.2.3 (a) is band-to-band or direct recombination. This transition occurs in room temperature and can be used to determine band gap energies of the materials. Band-to-band transition involves the recombination of free electrons and free holes and takes place when an electron falls from conduction band to the empty valance band associated with the hole.

Fig.2.3 (b) describes free exciton transition. Coulomb attraction between the electron and hole can lead to the formation of an excited state in which they are hold together. This state is referred as a free exciton (FE). Its energy is slightly smaller than the band gap energy. In a direct semiconductors, the energy of the emitted photon is;

$$h\nu = E_g - E_x \tag{2.34}$$

where E_g is the band gap energy of the material and E_x is the Coulomb energy of the exciton.

If the material has impurities then one of the possible transitions is the Bound Exciton (BE) which is illustrated in Fig. 2.3 (c) and (d). A free hole can combine with a neutral donor or a free electron can combine with a neutral acceptor both forming bound excitons.

Lastly, Fig.2.3 (e) shows donor-acceptor recombination. In this transition, an electron on a neutral donor recombine with a hole on a neutral acceptor. The recombination energy of a donor acceptor pair is modified by Coulomb attraction and then given by the following expression;

$$h\nu = E_g - (E_A + E_D) + \frac{q^2}{\epsilon r} \tag{2.35}$$

where E_g is the band gap energy, E_D and E_A are the binding energy of the donor and the acceptor and r is the distance between donor and acceptor.

CHAPTER 3

EXPERIMENTAL CONSIDERATIONS

3.1 Crystal Growth

Cooling a melt in a suitable container until it is solidified is one of the earliest methods used for the growth of large single crystals. One of the today's most commonly used methods have been developed starting with the work of Bridgman (1925) and Stober (1925). In Bridgman method crucible is moved relative to the temperature gradient whereas in Stober technique temperature gradient is moved relative to the stationary crucible. Kapitza showed that the process can be performed horizontally with the advantage that the top surface of the melt and crystal do not need to be in contact with the crucible [35].

The first step of the Bridgman technique is to determine a suitable growth ampoule, which is also called as crucible. In this case, one should consider the thermal expansion coefficient and melting point of the crystal that will be grown. Because of the contact between the crystal and particularly the solid-liquid interface with the crucible, surface of the crucible is very important. It should not contaminate with the grown material. Thus, the melting point of the ampoule must be higher so that the crucible material does not react with the melt and the solid. The thermal expansion coefficient of the crucible should be small compared

to that of the grown crystal. The crucible should have smaller thermal conductivity than the material it contains so that the solid-liquid interface isotherm has more appropriate shape to grow better quality crystals. As a result, quartz ampoules are used for preparing the crucibles for growth of many crystals having melting point below that of quartz [35].

We have used quartz crucibles as well. The crucible dimensions were 10-16 mm internal diameter and approximately 100 mm length with 1.5 mm wall thickness. The bottoms of the crucibles were conical in order to have desired nucleation and proceeding of a single crystal. The crucibles are usually contaminated by inorganic materials, surface dust and grease. These contaminations must be cleaned by a suitable manner prior to the growth process. Grease and dust were removed by brushing the crucibles with detergent and boiling water. Then we cleaned the growth ampoules chemically. Firstly, we kept the crucibles in a 40% HNO_3 solution to remove metallic impurities on the surface. Secondly, we cleaned them with detergent in an ultrasonic bath to remove the oil on the surface. Thirdly, we rinsed them with distilled water in an ultrasonic cleaner. Lastly, the crucibles were heated under vacuum up to 1000^oC in order to outgas the remaining impurities inside them. Following this processes, we cleaned the ampoules with detergent in an ultrasonic bath and rinsed with distilled water. Then they were left to dry [39].

The polycrystalline material is synthesized from $4N_s$-pure indium and $4N_s$-pure selenium shot in the ratio of 52% In and 48% Se. These elements were put into the cleaned crucible after they kept in acidic bath for a few minutes.

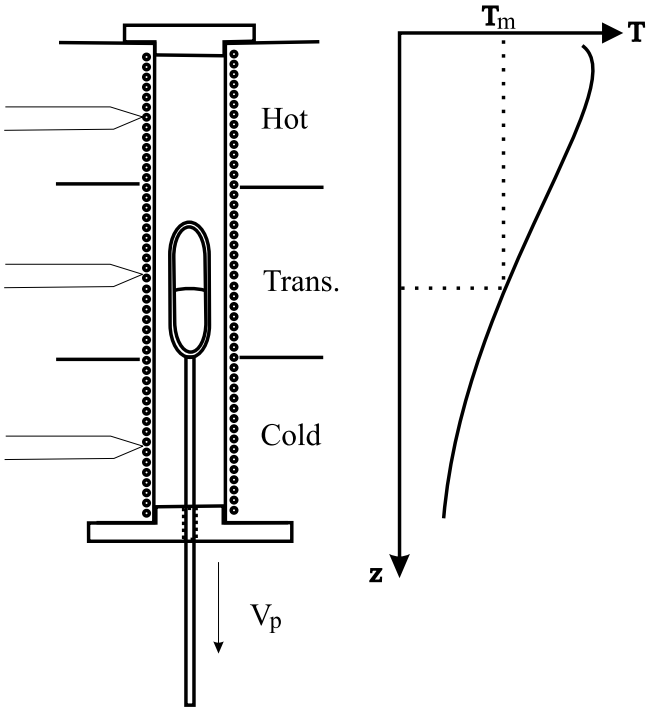

Figure 3.1: The furnace and ideal temperature distribution along the axis of a cylindrical crucible and heat flow in the crucible.

The ampoule was evacuated and sealed within a pressure of 10^{-5} torr. The ampoule was gradually heated up to 750^oC to let indium and selenium react. After the reaction, the compound was kept at 750^oC for 12 h and the ampoule was mechanically shaken at times to insure a complete reaction and homogeneity throughout the whole specimen. Since the vapor pressure of selenium is very high, we performed the heating process very carefully to avoid explosion of the ampoule. After synthesis, we cooled the furnace slowly to the room temperature.

We have grown InSe single crystals from non-stoichiometric melt using Crystalox MSD-4000 model 3-zone Vertical Bridgman-Stockbarger system in the Crystal Growth Laboratory of Physics Department. The illustration of the furnace

with a crucible and the temperature profile along the furnace can be both seen in Fig.3.1. Three independent heating zones, each 150 mm long, are included within the furnace. The zone names are upper zone, adiabatic zone and lower zone respectively. Three thermocouples adjacent to the center of each zone control the temperature inside the furnace. The temperatures of each zone are set by means of Eurotherm 902P programmable controllers and kept constant within an accuracy of 0.1^oC. The top of the furnace is closed by a ceramic plug to ensure temperature insulation. Another thermocouple is present at the tip of the furnace by means of which the user can provide the desired temperature profile prior to the growth process. In our system, there is also another thermocouple which alerts the user when the overheating takes place. If the overheating occurs, the whole system shuts down itself with alarm light and signal. Our system has Crucible Translation Unit (CRT) by means of which the loaded crucible is moved both upward and downward in appropriate speed.

The synthesized material was put into the prepared growth ampoule. The ampoule was placed to the upper part of the furnace. Then, we started the solidification process by moving the crucible from the hot zone to cold within a temperature gradient of 20^oC/cm, with the lowering speed 1 mm/h. The top zone, middle zone and bottom zone were set to 750, 450 and 250^oC, respectively. The axial thermocouple was used for monitoring the temperature at the tip of the crucible. The growth lasted nearly 160 hours with a lowering speed of 1 mm/h.

The stoichiometry of the grown crystal was examined by a JSM 6400 scanning electron microscope in the Department of Metallurgical and Material Engineering

at METU and the result show that our ingot was stoichiometric.

3.2 Implantation and Annealing

In ion implantation, ionized atoms are introduced onto the surface of a solid material by bombardment with ions in the keV to MeV energy ranges. In this technique, the concentration and distribution of implanted atoms can easily be controlled. However, the bombarded substrate might be damaged due to the collisions between implanted atoms and lattice atoms during the implantation. The damage introduced by ion implantation can be removed by means of annealing the samples. During annealing, the implanted atoms can be activated as well.

In our study, we used a Varian Model 200-DF4 type implanter in the Department of Physics at METU to implant the samples. This implanter has a gas box which contains dopant source. This source was ionized and then it was extracted into the acceleration tube in which the ions were accelerated to the specified kinetic energy. An analyzer was used to select solely the desired ion species. After focusing the ion beam to the targets, they were uniformly implanted using a scanning system.

The samples were cleaved from the ingot along the layers using a razor blade for the N-implantation. Sample dimensions and thickness were $4\times6\ mm^2$ and 150 μm respectively. The surfaces of the samples were then bombarded by nitrogen ion beam of 100 keV with the dose of $6\times\ 10^{15}$ ions/cm^2.

The total distance that an ion goes through a target material until it is stopped is called its range R. The projected range R_p is the projection of this distance

along the axis of incidence. The projected range of ion species of interest through a specified crystalline material can be estimated by using a computer program whose name is TRIM. It is a software included in the Stopping and Range of Ions in the Matter program (SRIM) including a group of programs using a quantum mechanical approach to the ion-atom interactions. TRIM statistically calculates some parameters like R_p and 3D distribution of ions using Monte Carlo algorithm [40]. Using TRIM calculation we estimated the distribution of the implanted ions and the result showed that the distribution of the implanted impurities had a gaussian shape through a projected range (R_p).

Implanted samples were annealed at 350 and 425^oC to remove the damages introduced by the implantation. As-grown samples were also annealed at 250, 350 and 450^oC to investigate the annealing effects on electrical, optical, and structural properties of InSe and the results were compared with that of the implanted samples.

3.3 Electrical Measurements

We carried out the temperature dependent electrical conductivity and Hall-effect measurements over the temperature range from 80 K to 400 K under vacuum in a Janis Liquid nitrogen cryostat using Lake-Shore 331 temperature controller. In the measurements we used Keitley 220 programmable constant current source and Keitley 619 electrometer. In the Hall-effect measurements a constant magnetic field of 0.97 T was applied parallel to the c-axis of the samples using Magnion FFC-4D magnets. Fig.3.2 illustrates the electrical conductivity and

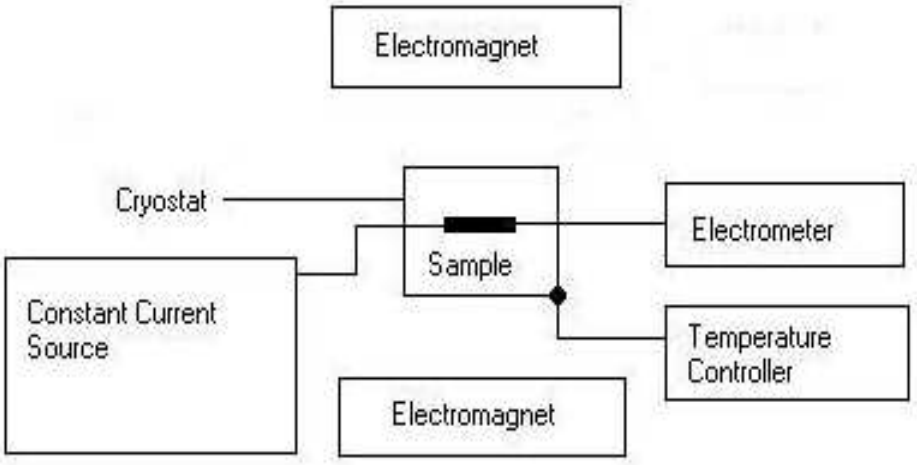

Figure 3.2: The Hall System.

Hall-effect set-up.

We made the electrical contacts for conductivity and Hall-effect measurements with indium by means of Nanotech thermal evaporation system in a vacuum of about 10^{-5}torr using appropriate masks. Electrodes were attached to contact region using silver paint. We observed the ohmic behavior of the contacts by the linear variations of the I-V characteristic, which is independent of the reversal of the applied bias in working current and temperature range. Fig.3.3 shows the Hall Bar contact geometry used in the conductivity and Hall-effect measurements.

For the conductivity and resistivity calculations, the current and voltage were measured through the contacts 1 and 3. In order to determine the Hall constant, a direct current was applied through the contacts 1 and 3 and the Hall voltage was measured between the contacts 2 and 4. We reduced the error which may be introduced by the thermoelectric effects by reversing the current, taking a second reading and averaging them. It is usually the case that there is a voltage between

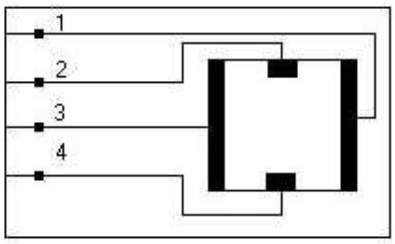

Figure 3.3: The sample geometry with the contacts

the contacts 2 and 4 in the magnetic field due to their imperfect alignment. We eliminated this error by reversing the magnetic field and measuring the Hall potential between the contacts 2 and 4 again. Averaging these four readings can reduce all random errors in Hall-effect experiments. We can find the Hall constant by using the following relation;

$$R_H = \frac{V_H t}{BI} \tag{3.1}$$

where V_H is the Hall voltage , t is the thickness of the sample, B and I are the applied magnetic field and current, respectively. We calculated the sample conductivity using the following equation:

$$\sigma = \frac{IL}{V\omega t} \tag{3.2}$$

where I is the applied current, V is the measured voltage, L, ω and t are the length, width and thickness of the sample, respectively.

3.4 Optical Measurements

We carried out absorption and Photoluminescence measurements at room temperature in the laboratories of the Department of Physics at Middle East

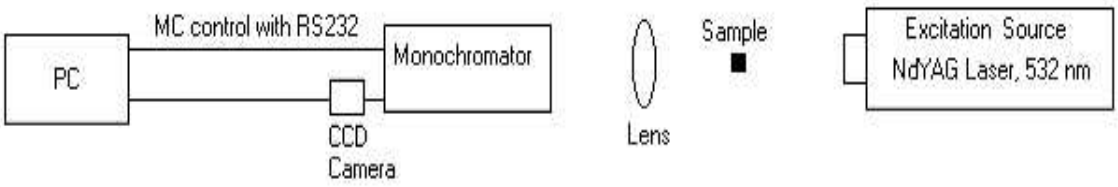

Figure 3.4: The PL setup.

Technical University.

For absorption measurements, we used Bruker made Equinox 55 model Fourier Transform Infrared (FT-IR) spectrometer with the resolution of 0.5 cm^{-1}. The spectrometer is computer supported and it is easy to obtain absorbance values against the wavelength using the software. We scanned the samples using the wavelengths between 700 and 1500 nm. The samples were placed in the holder such that the typical sample cross section was approximately 10 mm^2.

For PL measurements, the samples were cleaved from the ingot and their dimensions were about 1 cm^2 of area and 100 μm of thickness. The samples were excited using the 532 nm line of a NdYAG pulsed laser at room temperature. The energy of the laser (2.33 eV) was higher than the band gap energy of InSe ($\sim$1.3 eV). The average laser power was 0.3W. The luminescence was collected and detected by using a pair of lenses, mirror, monochromator, charge-coupling-devices (CCD) and computer. Fig.3.4 shows the PL setup.

3.5 Structural Measurements

X-ray crystallography is an experimental technique that exploits the fact that X-rays are diffracted by crystals. X-rays have the proper wavelength to be scattered by the electron cloud of an atom of comparable size. How X-rays are used

in the structural analysis of the crystal systems was mentioned in Chapter 2. We used Rigaku made powder diffractometer in the measurements. The system uses a target material so that the wavelength of interest is obtained and then scans the samples in the desired ranges between 0 and 180^o. We used Cu as the target material (Cu K_α= 1.5418 $\mathring{A}$) and scanned the samples between 5 and 80^o. The diffractometer is computer supported and the software provide us the qualitative analysis of the X-ray patterns.

CHAPTER 4

RESULTS AND DISCUSSIONS

4.1 Crystal Growth and Structural Analysis

We have successfully grown an ingot of InSe single crystal having a diameter of approximately 16 mm and length 30 mm. The samples were obtained by cleaving the ingot parallel to the layer which was perpendicular to the c-axis. We have performed X-ray measurements to determine the crystal structure using CuK_α radiation (λ =1.54059 A) in the scan range between 5^o and 80^o . The obtained 2θ values have been used in TREOR 90 which is a trial-and-error program for indexing of the patterns. The program involves separate routines for crystal symmetries and searches for possible solutions. Fig.4.1 shows the X-ray diffraction pattern of powdered as-grown InSe. The X-ray analysis of the powdered as-grown sample has shown that there is a preferred orientation along the c axis with the (004) direction. The observed reflection peaks of X-ray spectra can be referred to the typical (00ℓ) lines of the hexagonal structure of InSe. As a result of the analysis of X-ray pattern given in Fig.4.1 by TREOR 90, it was observed that the structure of the samples was hexagonal and lattice parameters a and c were 4.021 and 16.636 $\mathring{A}$ respectively. It was reported that the atoms inside each plane of InSe are arranged in rhombohedral or hexagonal modifications with lattice

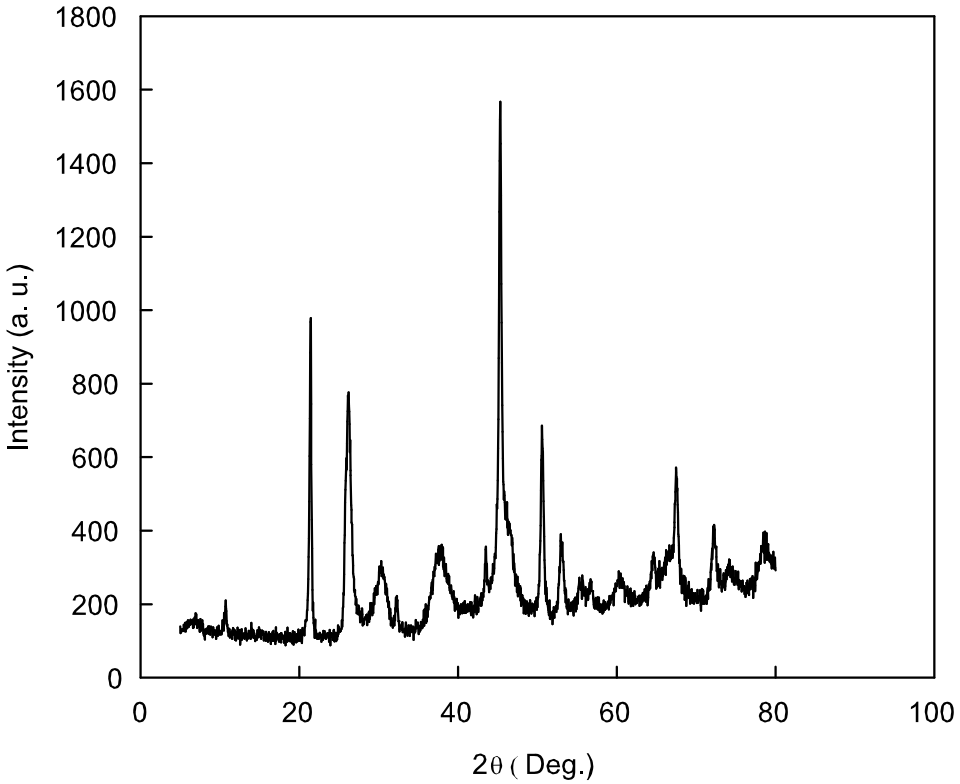

Figure 4.1: X-ray diffraction pattern of powdered as-grown InSe.

parameters a=4.005 $\mathring{A}$ and c=16.640 $\mathring{A}$ [9]. Our results were consistent with the ones given in JCPDS files. The card number for InSe in JCPDS files is 34-1431. Table 4.1 shows the relative intensities, crystal structure and lattice parameters of the observed reflections of InSe given in JCPDS data file.

Table 4.2 shows the relative intensities, crystal structure and lattice parameters of the observed reflections from our powdered as-grown InSe sample. We obtained eight diffraction maxima from the X-ray diffraction pattern of powdered InSe single crystals. All of the corresponding d values matched to the actual d values of InSe determined by S. Popovic et al. [11].

Fig.4.2 shows the XRD patterns of cleaved samples in the form of as-grown and annealed at 350 and 425^{o}C, respectively. As it can be seen from the figure,

Table 4.1: JCPDS information for InSe [41].

Structure:Hexagonal Unit cell volume=266.906 $(\mathring{A})^3$ a=4.005 $\mathring{A}$ b=4.005 $\mathring{A}$ c=16.640 $\mathring{A}$	parameters	
h k l	d($\mathring{A}$)	I/I_0
0 0 2	8.32	16
0 0 4	4.17	100
1 0 0	3.465	2
1 0 1	3.410	2b
1 0 3	2.940	3b
0 0 6	2.773	10
1 0 5	2.400	3b
0 0 8	2.080	8
1 1 0	2.00	4
1 0 7	1.970	2b
1 1 4	1.805	2
2 0 1	1.728	1
0 0 -10	1.663	<1
1 1 6	1.623	1
2 0 5	1.536	<1
1 1 8	1.443	1
0 0 -12	1.386	12
2 1 1	1.307	<1
0 0 -14	1.187	1
3 0 0	1.156	<1
1 1 -12	1.140	3
0 0 -16	1.039	2
1 1 -14	1.023	<1
2 2 0	1.001	<1
0 0 0-18	0.924	1

Table 4.2: TREOR 90 output from the x-ray measurement of powdered as-grown InSe.

Structure:Hexagonal Unit cell volume=268.98 $(\AA)^3$ a=4.021 $\AA$ b=4.021 $\AA$ c=16.636 $\AA$	parameters			
h k l	2 θ obs.	2 θ cal.	d(Å)	I/I_0
0 0 2	10.627	10.627	8.3180	14
0 0 4	21.340	21.347	4.1604	100
1 0 1	26.122	26.122	3.4086	13
0 0 6	32.249	32.260	2.7736	11
0 0 8	43.484	43.484	2.0795	14
1 1 0	——	45.054	——	24
1 1 4	50.563	50.369	1.8037	11
0 0 12	——	67.509	——	20

the peak positions of the annealed samples are in agreement with the as-grown sample but the intensities of the peaks decrease with annealing. This is due to the fact that crystals behave like amorphous materials when they are annealed at high temperatures that is the result of decreasing crystallinity and increasing structural disorder with post annealing. As the annealing temperature increases, sheet defects like stacking faults and segregation results in the structural disorder in the crystal.

Fig.4.3 shows the XRD patterns of as-grown, N-implanted, and annealed at 350 and 425^{o}C samples, respectively. It can be seen from the figure that the reflection intensities of implanted sample decrease whereas the peak positions does not change. However, annealing following to the growth increases the intensities of the reflection peaks. This is actually the indication of structural deformation due to the introduced N impurities after implantation processes. As previously stated, the damage introduced by ion implantation can be reduced by annealing.

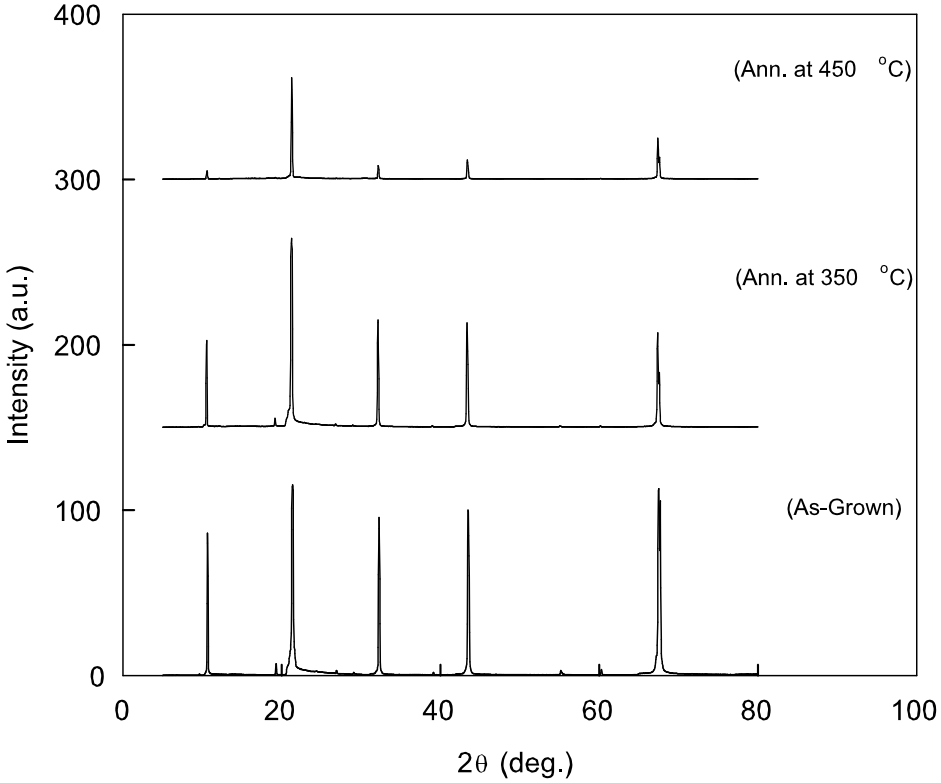

Figure 4.2: X-ray diffraction patterns of as-grown and annealed at 350 and 450^{o}C InSe samples. Patterns are shifted upward for the sake of clearance.

Thus, the increasing reflection intensities of implanted sample with post annealing imply increasing crystallinity and decreasing structural disorder. This is indeed due to the diffusion of the ions into the deeper layers of the substrate.

4.2 Electrical Conductivity

Dark electrical measurements were carried out in the temperature range of 80-400 K. The contacts were made as described in chapter 3. Linear variations of the I-V characteristic have shown that our contacts had ohmic behavior.

We found the resistivity values of undoped (A0) samples perpendicular to c-axis to be around $1.8\times10^3\Omega$-cm at room temperature. This result is consistent with the order given in the literature [9]. It has been observed that conductivity

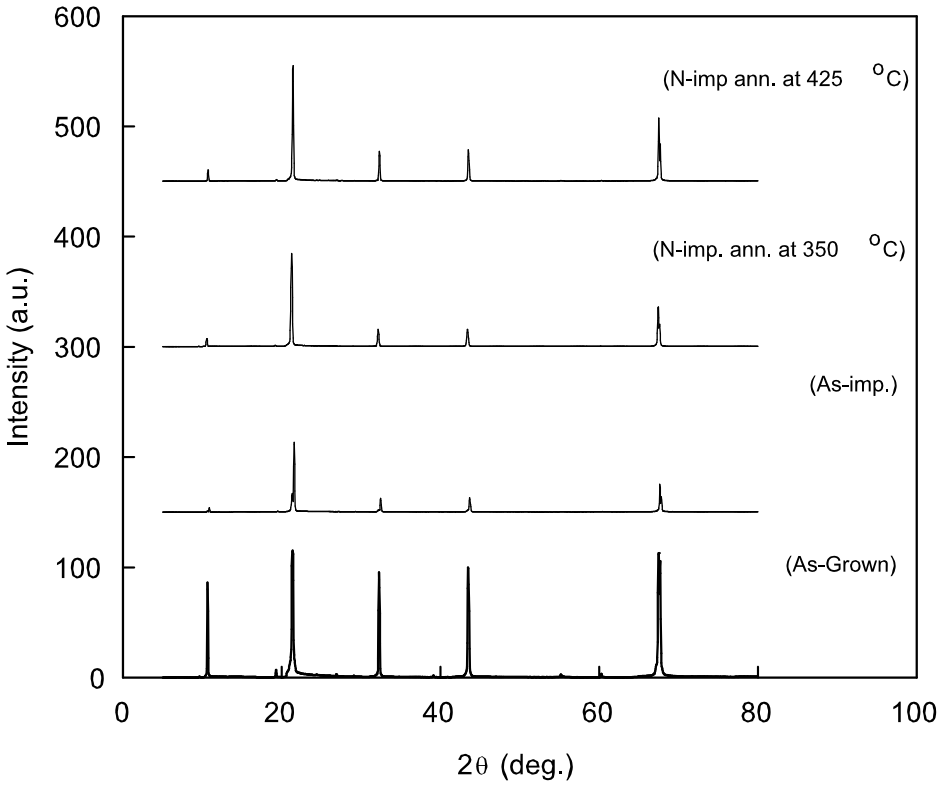

Figure 4.3: X-ray diffraction patterns of as-grown, N-implanted, N-implanted and annealed at 350 and 425^oC samples. Patterns are shifted upward for the sake of clearance.

shows an exponential dependence with temperature in the studied range. In low temperature region, the variation of the conductivity with temperature increases slowly, whereas in the high temperature region, the increase of the conductivity is much more pronounced. Such a conductivity variation may be useful to investigate the transport properties of the samples in the following manner. If $\ln(\sigma)$ is plotted with respect to 1/T, we can obtain the activation energy of the carriers from the slope of the graph in the linear temperature region. The temperature dependent conductivity is governed by the thermal excitation of electrons from levels in the forbidden gap to the conduction band. Thus, following the above considerations, the activation energies of the as-grown sample calculated from

the dark conductivity relation were 8 and 44 meV within the temperature ranges 100-140 and 170-250 K, respectively. We could not observe reasonable conductivity variations above 250 K. The activation energies of the investigated samples are relatively small compared to the literature [15, 17] that may be the results of imperfections existing in the structure. Therefore, it may be concluded that the trapping levels which are very close to the conduction and/or valance band are present in as-grown samples exhibiting metallic behavior with post annealing, which might be attributed to the increase of the structural deformations, presence of segregation and production of large stacking faults in the crystals. Fig.4.4 shows the temperature dependent dark conductivity of as-grown (A0), as-grown and annealed at 250^{o}C (A1) InSe crystals.

InSe single crystals were doped by N-atoms using the ion implantation technique. The samples were annealed to remove the damage introduced by the implantation and activate N doping centers. Dark electrical conductivity measurements were performed for as-implanted, implanted and annealed at 350^{o}C samples. The thickness of the implanted layers was estimated as 0.3 μm using TRIM calculation and it has been used as an effective thickness in the conductivity calculations of the implanted samples.

The room temperature resistivity value of undoped (A0) sample was $1.8\times10^3\Omega$-cm while the resistivity for N-implanted (B0) sample was found to be 2.5 Ω-cm. Doping with nitrogen by ion implantation reduced the resistivity of InSe single crystals. The activation energies calculated from the dark conductivity were 12 and 147 meV within the temperature ranges 160-200 and 210-350 K, respectively.

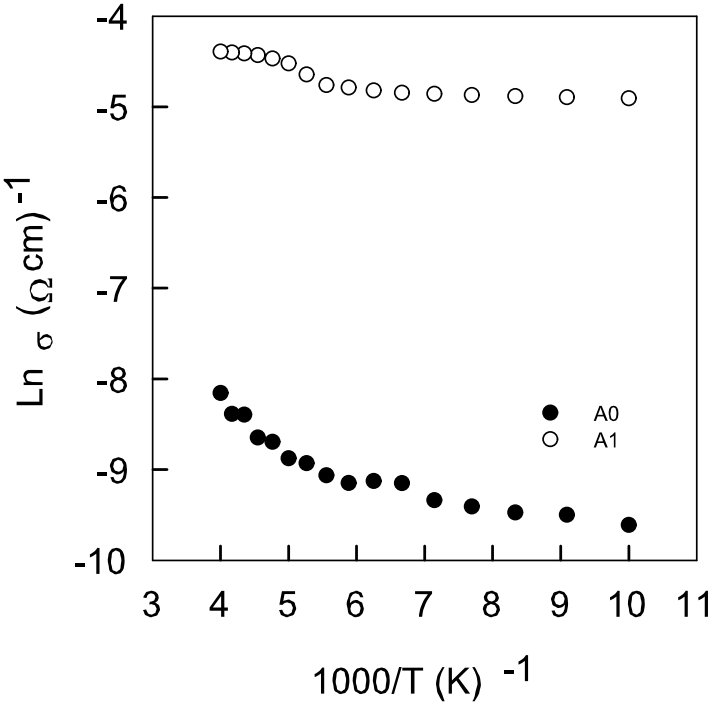

Figure 4.4: The temperature dependent conductivity of as-grown (A0) and annealed at 250 ^{o}C (A1) InSe samples.

These activation energies are higher compared to as-grown samples. These increases of activation energies imply that addition of N atoms through the crystal sweeps out the disorder existing in the InSe structure. Although this result seems to be inconsistent with what was stated in the structural analysis of the samples, the fact that X-rays travel many layers through the specimen whereas conductivity phenomenon takes place within the effective thickness of the implanted samples should be remembered.

Annealing of the implanted samples at and above 350^{0}C weakens the temperature dependence of the conductivity, which implies that the annealing of the samples activates N-atoms and causes structural modifications and changes in the stacking sequences. Fig.4.5 shows the temperature dependent dark conductivity of

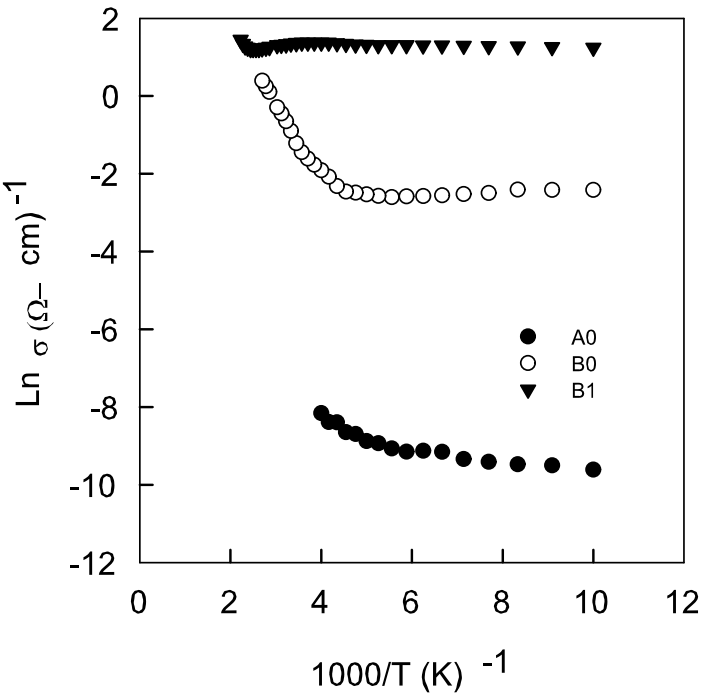

Figure 4.5: The temperature dependent conductivity of as-grown (A0), N-implanted (B0), implanted and annealed at 350 ^{o}C (B1) InSe samples.

as-grown (A0), as-implanted (B0), implanted and annealed at 350^{o}C (B1) InSe crystals.

4.3 Hall Mobility

The temperature dependent Hall mobility of the as grown and N- implanted InSe samples were performed as described in chapter 3. Our as-grown InSe samples had n-type conduction, which was verified by the Hall-effect measurements. We calculated the mobility values using the expression $\mu_H = \sigma R_H$. The Hall mobility of the as-grown sample was found to be 70 $cm^2/V.s$ at 250 K. Hall mobility was plotted as a function of temperature on a log-log scale. Fig.4.6 shows Hall mobility-temperature variations of as-grown sample (A0). In this plot, it is possible to detect the dominant scattering mechanisms assuming a relation $\mu \propto T^{\pm n}$,

where n is the temperature exponent, as described in chapter 2. We found n to be around 2 at lower temperature range and such a behavior actually is characteristic of a scattering mechanism of charge carriers with ionized impurities. In the higher temperature range (T>250 K), n should be around -1.5 theoretically, which indicates that the scattering of electrons is mainly due to the phonon scattering [18]. However, we could not obtain the reasonable data in conductivity measurements above 250 K.

Fig.4.7 shows the mobility dependence of N-implanted sample (B0) in log-log scale. The mobility of N-implanted sample at room temperature was found to be around $5\times\ 10^3$ cm$^2/V.s$. In low temperature region between 100 and 200 K, the n value was found to be -1.34 and the mobility decreased with increasing temperature reaching a minimum value $5\times\ 10^2\ cm^2/V.s$ at 160 K. Such a behavior was reported by A. Segura et al.[42] for a non-stoichiometric p-type InSe. In their report, it was stated that the type of the material changed from n to p unlike our results. Similar behavior was observed in [3] for N-implanted and annealed at 700^{o}C Bridgman grown GaSe samples. In our sample, the mobility increased with increasing temperature above 200 K reaching a value $17\ \times\ 10^3$ cm$^2/V.s$ at 350K.

In this temperature range, we found the n value as 3.62 which might be due to the high concentration of sheet defects, like stacking faults, behaving as shallow donor or acceptor levels in layered structures [3, 43]. Large n value may also indicate the low structural quality of the grown crystal and the structural deformations introduced by N atoms. The sheet defects in layered structures may

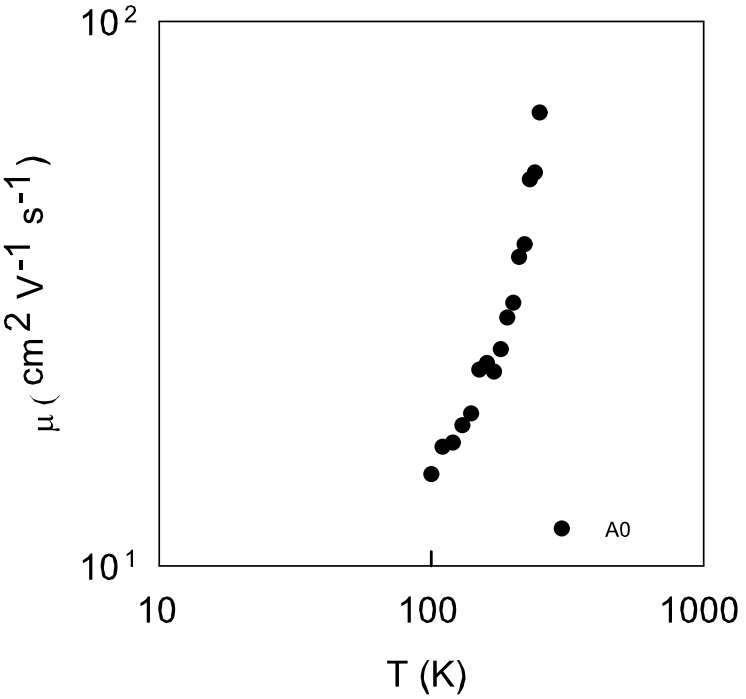

Figure 4.6: Mobility-temperature dependence of the as-grown sample (A0).

cause the lattice scattering mechanisms to compensate and the carrier mobility to increase after a critical temperature. Thus, the mobility variation with respect to temperature can be thought as to be governed by the structural defects.

4.4 Optical Absorption

Optical absorption or transmission measurements are commonly used techniques to find the optical absorption coefficient, band structure and impurity levels of the materials. In these techniques, light is incident onto the sample and the transmitted light is measured as a function of wavelength. In the measurements we have used the FT-IR system.

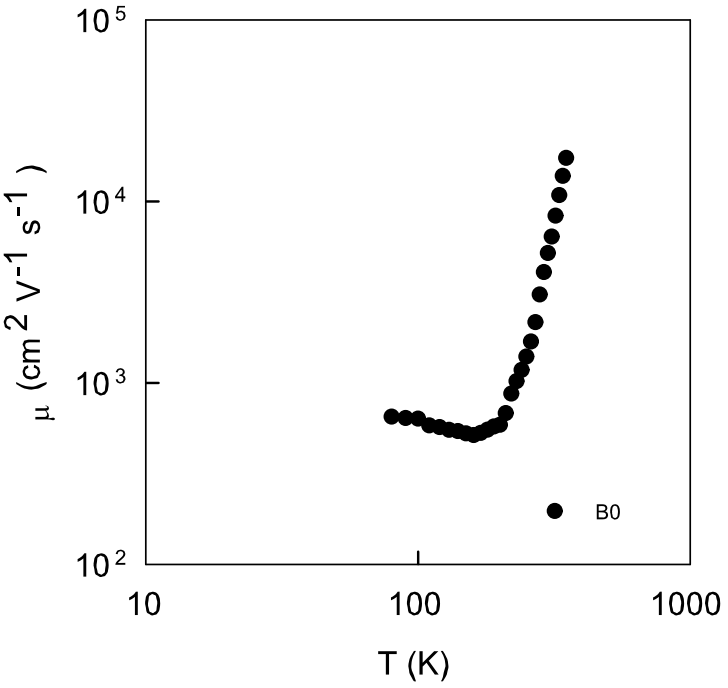

Figure 4.7: Mobility-temperature dependence of the as-implanted sample (B0).

Absorption coefficient can be expressed as follow [38];

$$(\alpha h\nu) = A(h\nu - E_g \pm E_p)^n \tag{4.1}$$

where A is a coefficient stemming from the transition probability, E_g is the band gap energy, E_p is the phonon energy which is equal to zero for direct transitions, and n is an index having values 1/2, 3/2, 2 and 3. If n is 1/2 or 3/2 then the transition is said to be direct, otherwise it is indirect. Fig.4.8 shows the optical absorption spectrum of as-grown InSe (A0) at room temperature. One can see from the figure that $(\alpha$ h $\nu)^2$ vs hν gave a straight line. We performed the transmission measurements at room temperature and α is in the order of $10^3 \mathrm{cm}^{-1}$. Thus, exciton is not possible in our case. Consequently, we can assign a value 1/2 to n and the absorption is due to the direct transition from the valance

band to the conduction band. We determined the band gap energy of as-grown sample from the intercept and it was around 1.22 eV at room temperature for undoped InSe. Fig. 4.8 shows the optical absorption spectrum of as-grown InSe (A0).

In order to see the annealing effect on absorption spectra, we backed the samples at different temperatures. Fig.4.9 shows the absorption spectrum of as-grown (a), annealed at 250^{o}C (b), and annealed at 350^{o}C (c) InSe samples. No considerable changes have been observed on the absorption spectra of undoped InSe single crystals with post annealing.

The absorption spectrum for N- implanted (a), annealed at 250^{o}C (b), and annealed at 350^{o}C (c) InSe samples are presented in Fig.4.10. We carried out the transmission measurements at room temperature and the band gap energy of the implanted sample was found to be around 1.22 eV. The band gap energies found for both the as-grown and as-implanted samples are in agreement with the literature [9, 31]. Annealing exhibited no considerable change on the absorption spectrum of the implanted samples.

4.5 Photoluminescence

Photoluminescence (PL) spectroscopy is a very powerful tool in order to determine the band gap, impurity levels and defects of a semiconductor. It is also possible to obtain information about the recombination mechanisms in the crystals by performing PL measurements. Fig.4.11 shows the PL spectrum of as-grown (a) and annealed at 250^{o}C (b) InSe single crystals at room temperature.

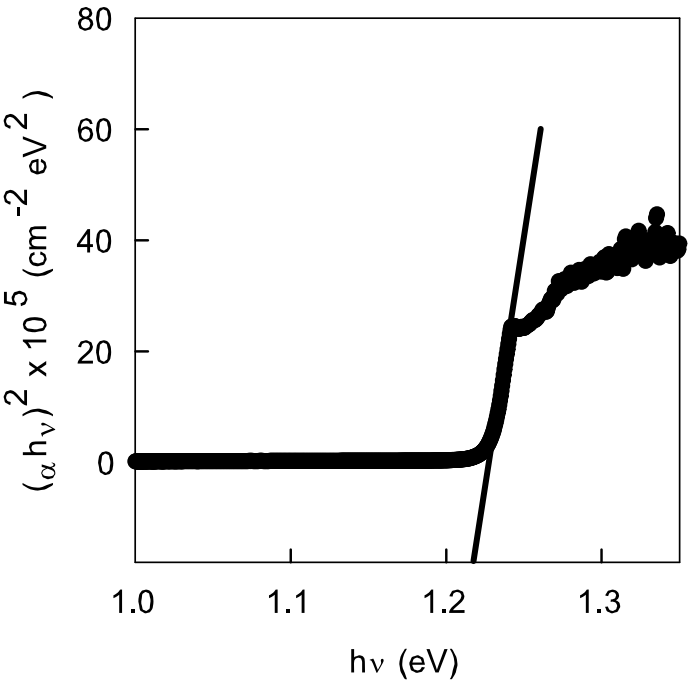

Figure 4.8: Optical absorption spectrum of as-grown InSe (A0) at room temperature.

The band gap energies determined from the PL spectrum were around 1.23 and 1.24 eV for as-grown and annealed at 250^{o}C samples, respectively. These values are in agreement with the ones given in [9, 31]. Annealing exhibited almost no effects on PL spectrum of as-grown samples. We could not obtain PL spectrum for the implanted samples.

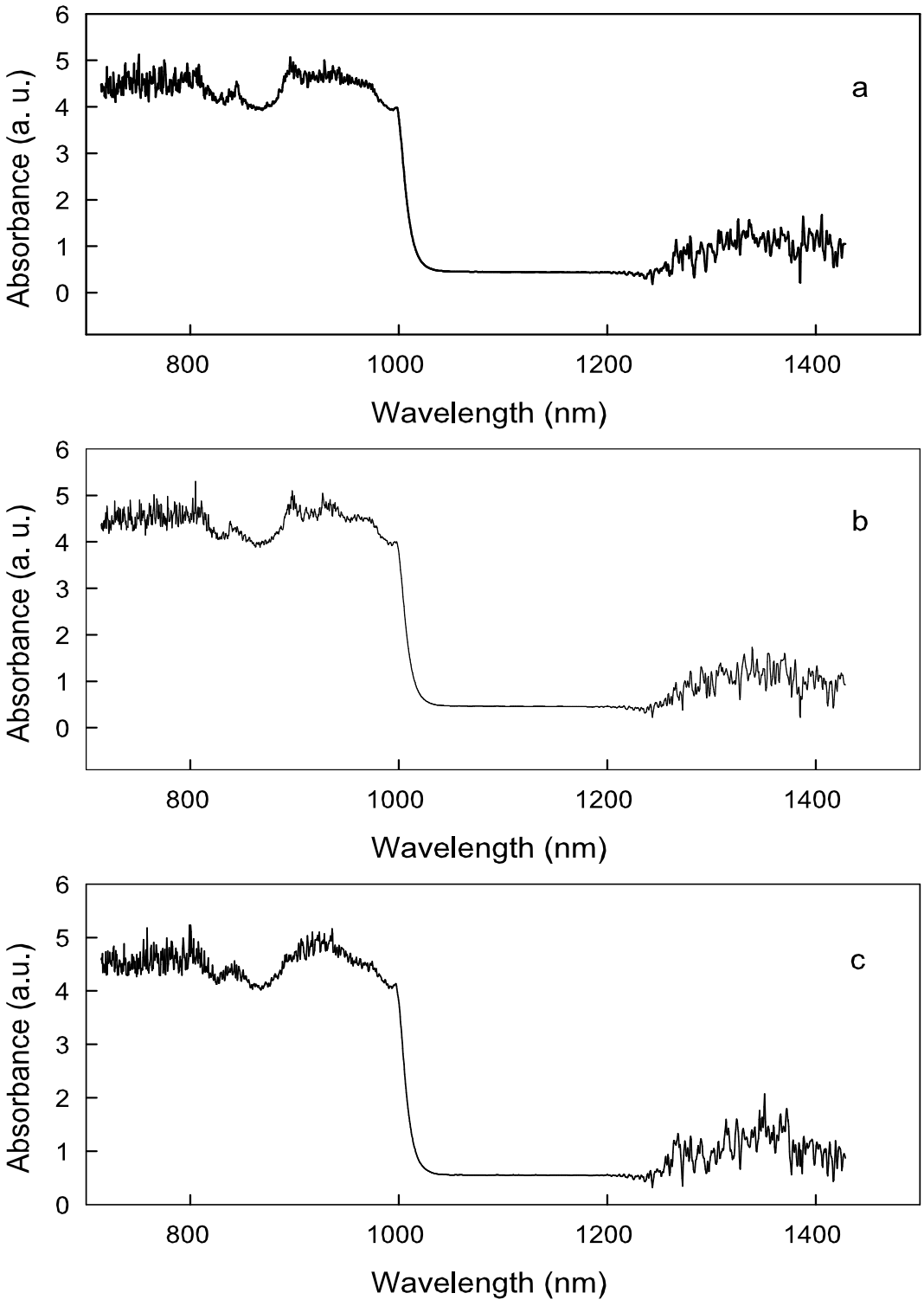

Figure 4.9: The absorption spectrum of as-grown (a), annealed at 250^{o}C (b), and annealed at 350^{o}C (c) InSe samples.

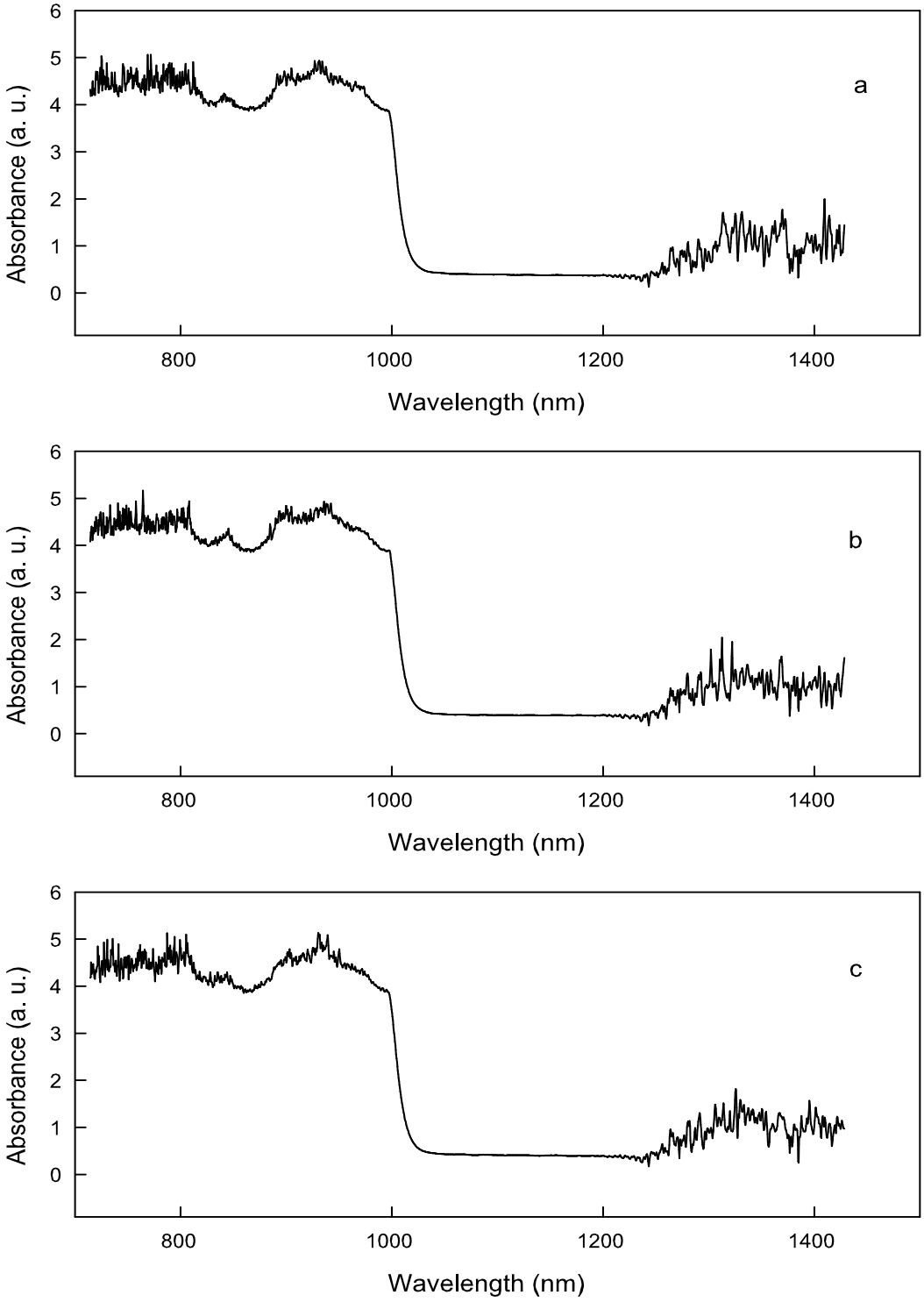

Figure 4.10: The absorption spectrum of as-implanted (a), annealed at 250^{o}C (b), and annealed at 350^{o}C (c) InSe samples.

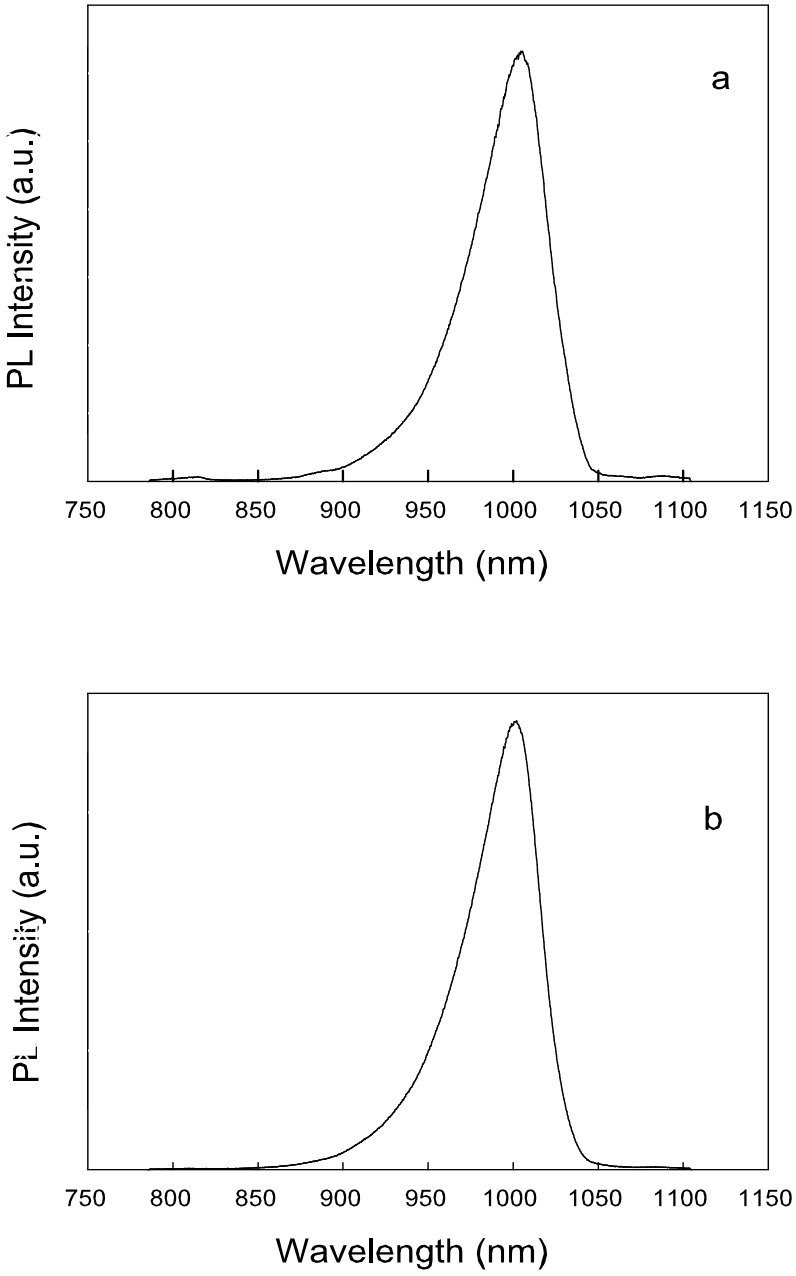

Figure 4.11: The PL spectrum of as-grown (a) and annealed at 250^{o}C (b) InSe samples.

CHAPTER 5

CONCLUSION

In this study, we have grown indium monoselenide single crystals using conventional 3-zone Bridgman-Stockbarger directional solidification system. We let the crystal grow in a 20^{o}C/cm temperature gradient with a pulling speed of 1mm/h. In order to determine the doping effect on Inse, as-grown samples were implanted by N atoms. The surfaces of the samples were bombarded by nitrogen ion beam of 100 keV with the dose of 6×10^{15}/cm ^{2}. We examined the as-grown and implanted samples considering their structural, electrical and optical properties.

The peak positions found from XRD pattern of the as-grown samples were the same as those of as-implanted and annealed samples. However, the intensities of the peaks were more intense in as-grown samples compared to as-implanted samples. Thus, we concluded that implantation reduced the crystallinity of the as-grown samples. From the analysis of the XRD patterns of as-grown, as-implanted and annealed samples, we observed that there was a preferred orientation along the c-axis with the (004) direction for all of the samples. The increasing peak intensities in this direction with annealing showed increasing crystallinity in implanted samples. The surface morphology of the samples was determined with a JSM 6400 scanning electron microscope. It was concluded that our ingot was

stoichiometric.

The temperature dependent dark electrical conductivity measurements along the layers were carried out for both as-grown and as-implanted samples. We observed that N-implantation reduced the resistivity values from $1.8\times10^3\Omega$-cm to 30 Ω-cm at room temperature. For the as-grown samples, the activation energies calculated from the conductivity relation were 8 and 44 meV within the temperature ranges 100-140 and 170-250 K, respectively. For the as-implanted samples, the activation energies were found to be 12 and 147 meV within the temperature ranges 160-200 and 210-350 K, respectively. This result showed that addition of N atoms through the crystal sweeps out the disorder existing in the InSe structure. The conductivity variations of as-grown and as-implanted samples were actually very small in magnitude and both as-grown and as-implanted samples gained metallic behavior with post annealing. This result might be attributed to the fact that our crystals were not good in quality. In order to enhance the crystal quality, higher temperature gradients might be used with lower pulling rates as suggested in the literature [9, 20, 21]. We could not achieve a temperature gradient in these ranges in our Bridgman system.

We performed temperature dependent Hall Effect measurements of the as-grown and as-implanted samples. The temperature dependent mobilities of these samples obeyed the power law $\mu \propto T^{\pm n}$ with different n values. The mobility of the as-grown sample was found to be 70 $cm^2/V.s$ at 250 K. The room temperature mobility of the as-implanted sample was around $5\times\ 10^3$cm^2/V.s. For the as-grown sample, the Hall mobility is limited by ionized impurity scattering at lower

temperature range below 250 K. The conductivity variation above 250 K did not let us determine the scattering mechanism but at higher temperature range above 250 K the scattering of electrons should have been mainly due to the phonon scattering as it is stated by C. De Blassi et al. [18]. The Hall mobility of the as-implanted sample was limited by phonon scattering at lower temperature range while the scattering of electrons was due to the ionized impurity scattering at higher temperature range above 200 K.

From the absorption and photoluminescence measurements at room temperature, we have tried to figure out the annealing effect on the band gap energy of both undoped and implanted samples. From absorption measurements the band gap energies were found to be 1.22 for both as-grown and as-implanted samples, respectively. Annealing did not change the absorption spectrum of the as-grown and as-implanted samples. From the PL measurements, the band gap energies were found to be around 1.23 and 1.24 eV for the as-grown and annealed at 250^{o}C samples, respectively. For the as-grown samples, the obtained band gap energy values from both PL and absorption measurements were comparable to each other.

REFERENCES

[1] C. Kittel, Introduction to Solid State Physics (Jhon Wiley and sons,Inc., New Jersey, 1962).

[2] M. Shur, Introduction to Electronic Devices (John Wiley and sons,Inc., New York, 1996).

[3] O. Karabulut, Structural, electrical and optical characterization of N- and Si-implanted GaSe single crystal grown by Bridgman method (Ph. D. thesis, METU, 2004).

[4] M. K. Anis and F. M. Nazar, J. Mater. Sci. Lett., 2, 471, (1983).

[5] S. Shigetomi, T. Ikari, and H. Nakashima, Phys. Stat. Sol.(b), 209, 93, (1998).

[6] T. Ishii, J. Crystal Growth, 89, 459, (1998).

[7] O. Kararbulut, M. Parlak, R. Turan, U. Serincan, E. Tasarkuyu, and B. G. Akinoglu, Crystal Res. and Techn., 38(9), 811, (2003).

[8] O. Karabulut, M. Parlak, K. Yilmaz, R. Turan, and B. G. Akinoglu, Crystal Res. and Tech., 38(12), 1071, (2003).

[9] C. De Blassi, G. Micocci, S. Mongelli, A. Tepore, and F. Zuanni, Materials Chemistry and Physics, 9, 55, (1983).

[10] C. De Blassi, G. Micocci, S. Mongelli, and A. Tepore, J. Crystal Growth, 57, 482, (1982).

[11] S. Popovic, A. Tonejc, B. Grzeta-Plenkovic, B. Celustka, and R. Trojko, J. Appl. Cryst., 12, 416, (1979).

[12] A. Segura, J. P. Guesdon, J. M. Besson, and A. Chevy, J. Appl. Phys., 54(2), 876, (1983).

[13] C. De Blassi, G. Micocci, A. Rizzo, and A. Tepore, Phys. Stat. Sol.(a), 74, 291, (1982).

[14] T. Ikari and S. Shigetomi, Phys. Stat. Sol.(b), 124, K49, (1984).

[15] P. I. Savitskii, Z. D. Kovalyuk, and V. Mintyanskii, Phys. Stat. Sol.(a), 180, 523, (2000).

[16] R. Cingolani, L. Vasanelli, and A. Rizzo, Il Nuevo Cimento, 6(5), 383, (1985).

[17] S. Shigetomi, T. Ikari, Y. Koga, and S. Shihetomi, Phys. Stat. Sol.(a), 86, K69, (1984).

[18] C. De Blassi, G. Micocci, A.Rizzo, and A. Tepore, Physical Rewiev B, 27(4), 2429, (1983).

[19] P. I. Savitskii, I. V. Mintyanskii, and Z. D. Kovalyuk, Phys. Stat. Sol.(a), 155, 451, (1996).

[20] A. Chevy, J. Crystal Growth, 67, 119, (1984).

[21] A. Chevy, A. Kuhn, and M. S. Martin, J. Crystal Growth, 38, 118, (1977).

[22] A. A, Homs and B. Mari, J. Appl. Phys., 88(8), 4654, (2000).

[23] G. Micocci, A. Teopre, R. Rella, and P. Siciliano, J. Appl. Phys., 71(5), 2274, (1992).

[24] G. Micocci, M. Molendini, A. Tepore, R. Rella, and P. Siciliano, J. Appl. Phys., 70(11), 6847, (1991).

[25] S. Shigetomi and T. Ikari, Jpn. J. Appl. Phys.1, 42(11), 6951, (2003).

[26] G. Micocci, A. Tepore, R. Rella, and P. Siciliano, Phys. Stat. Sol.(a), 133, 421, (1992).

[27] G. Micocci, A. Tepore, R. Rella, and P. Siciliano, Phys. Stat. Sol.(a), 128, K33, (1991).

[28] F. J. Manjon, Y. Van De Vijyer, A. Segura, V. Munoz, Z. X. Liu, and C. Ulrich, Phys. Stat. Sol.(b), 211, 105, (1999).

[29] G. Micocci, A. Tepore, R. Rella, and P. Siciliano, J. Appl. Phys., 78(9), 5427, (1995).

[30] M. Yildirim, B. Gurbulak, B. Abay, H. Efeoglu, S. Tuzemen, and Y. K. Yogurtcu, J. Appl. Phys., 80(8), 4437, (1996).

[31] S. Shigetomi and T. Ikari, J. Appl. Phys., 93(4), 2301, (2003).

[32] J. Riera, A. Segura, and A. Chevy, Phys. Stat. Sol.(a), 142, 265, (1994).

[33] V. Vladimir, V. Gridin, C. Kasl, J. D. Comins, and R. Beserman, J. Appl. Phys., 71(12), 6069, (1992).

[34] I. V., Markov, Crystal Growth for Beginners (Singapore, 1998).

[35] J. C. Brice, Crystal Growth Processes (NY, 1986).

[36] B. D. Cullity, Elements of X-Ray Diffraction (Addison-Wesley, Second Edition, 1978).

[37] P. E. Werner, L. Eriksson, and M. Westdahl, J. Appl. Cryst., 18, 367, (1985).

[38] J. I. Pankove, Optical Processes in Semiconductors (Prentice-Hall Inc., London, 1971).

[39] J. J. Gilman, The Art and Science of Growing Crystals (John Wiley and sons,Inc., London, 1963).

[40] J. F. Ziegler, SRIM: The Stopping and Range of Ions in Matter, Program Manual (1996).

[41] JCPDS, International Center for Diffraction Data (1988).

[42] A. Segura, C. Martinez-Thomas, A. Casonovas, A. Martinez-Poster, and A. Chevy, Appl. Phys. A, 48, 445, (1989).